# Late Cretaceous to Paleocene oroclinal bending in the central Pontides (Turkey)

Maud J.M. Meijers, Nuretdin Kaymakci, Douwe J.J. Van Hinsbergen, Cor G. Langereis, Randell Stephenson, Jean-Claude Hippolyte

# Late Cretaceous to Paleocene oroclinal bending in the central Pontides (Turkey)

Maud J. M. Meijers,[1,2] Nuretdin Kaymakci,[3] Douwe J. J. van Hinsbergen,[1,4] Cor G. Langereis,[1] Randell A. Stephenson,[5] and Jean-Claude Hippolyte[6]

Received 2 October 2009; revised 27 February 2010; accepted 18 March 2010; published 3 August 2010.

[1] The Turkish Pontide fold-and-thrust belt formed since the Paleozoic and is an important element in the Africa-Eurasia convergence and the resulting closure of the Neo-Tethys ocean. It has a peculiar arc-shaped geometry in its central part, along the Black Sea coast, which may have resulted from oroclinal bending. We have determined the vertical-axis rotation history of this area using paleomagnetism on Cretaceous to Eocene rocks from 47 sites and critically analyzed previously published data. We applied the same reliability criteria to all data. Our results show that late Cretaceous sites have clockwise and counterclockwise rotations perpendicular to the structural trend in the central Pontides. In the eastern Pontides, they show only local rotations. Paleocene to Eocene rocks in the central and eastern Pontides show no rotation. We conclude that the central Pontide northward arc-shaped geometry results from oroclinal bending in latest Cretaceous to earliest Paleocene times. The timing and scale of geological processes that occurred in the region make it likely that orocline formation resulted from Neo-Tethys closure between the Pontides and the metamorphic promontory of the Anatolide-Tauride Block. Earlier studies on the southerly located Çankırı Basin reveal that clockwise and counterclockwise rotations occurred in Eocene-Oligocene times. This implies that the entire region underwent continuous deformation from late Cretaceous to Eocene, caused by convergence of the Pontides and the Anatolide-Tauride Block, with a southward moving deformation front. Deformation was first localized in the northern part of the central Pontides until the Paleocene, resulting in oroclinal bending, and from at least Eocene times it shifted toward the Çankırı Basin region. **Citation:** Meijers, M. J. M., N. Kaymakci, D. J. J. van Hinsbergen, C. G. Langereis, R. A. Stephenson, and J.-C. Hippolyte (2010), Late Cretaceous to Paleocene oroclinal bending in the central Pontides (Turkey), *Tectonics*, *29*, TC4016, doi:10.1029/2009TC002620.

## 1. Introduction

[2] The Turkish Pontides constitute a fold-and-thrust belt formed since the Paleozoic as a result of subduction and accretion processes during the closure of the Paleo-Tethys and Neo-Tethys oceans at the southern Eurasian margin [*Okay et al.*, 2006; *Şengör and Yilmaz*, 1981]. The Pontides were separated from Eurasia by the opening of the Black Sea basin during Cretaceous-Eocene times (Figure 1a) [*Görür*, 1988; *Hippolyte et al.*, 2010; *Okay et al.*, 1994; *Robinson et al.*, 1996; *Tüysüz*, 1999]. To the south, the Pontides are separated from the Pan-African Anatolide-Tauride Block by the İzmir-Ankara-Erzincan (IAE) suture zone, which represents the location of closure of the Neo-Tethys [*Şengör and Yilmaz*, 1981]. Collision between the Pontides and the Anatolide-Tauride Block took place in the late Cretaceous to Paleocene, with a final phase in the Eocene [*Görür et al.*, 1984; *Kaymakci et al.*, 2009; *Rice et al.*, 2006; *Şengör and Yilmaz*, 1981].

[3] The general east-west trend of the Pontide fold-and-thrust belt is disrupted in its central part by a peculiar northward convex geometry along the central Black Sea coast (Figure 1b). This central Pontides geometry could be original, having developed during initial nappe stacking or may represent a younger phase of oroclinal bending [*Carey*, 1958]. Oroclinal bending would require major, regional deformation of the pre-existing east-west striking fold-and-thrust belt. Such a distinct deformation event after a long-lasting process of subduction-accretion along the southern Eurasian margin may help identifying major changes in the geodynamic evolution of the closure of the Neo-Tethys, and roles of continent-continent collision, and the opening of the Black Sea.

[4] In this study we first test whether the northward convex geometry in the Pontides can be defined as an orocline. To do this, we have collected paleomagnetic samples from 47 sites in the central and eastern Pontides from lower Cretaceous to Eocene rocks to determine the vertical-axis rotation history of the region. In addition, we constrain the timing of rotations to enable correlation to large-scale geodynamic processes, by determining vertical-axis rotations in rocks taken from a sufficiently large time span (Cretaceous-Eocene). We have

[1]Paleomagnetic Laboratory Fort Hoofddijk, Department of Earth Sciences, Utrecht University, Utrecht, Netherlands.
[2]Department of Tectonics and Structural Geology, Faculty of Earth and Life Sciences, University of Amsterdam, Amsterdam, Netherlands.
[3]Department of Geological Engineering, Faculty of Engineering, Middle East Technical University, Ankara, Turkey.
[4]Physics of Geological Processes, University of Oslo, Oslo, Norway.
[5]School of Geosciences, University of Aberdeen, Aberdeen, UK.
[6]CEREGE, UMR 6635, Université Aix-Marseille III, CNRS, Aix-en-Provence, France.


0278-7407/10/2009TC002620

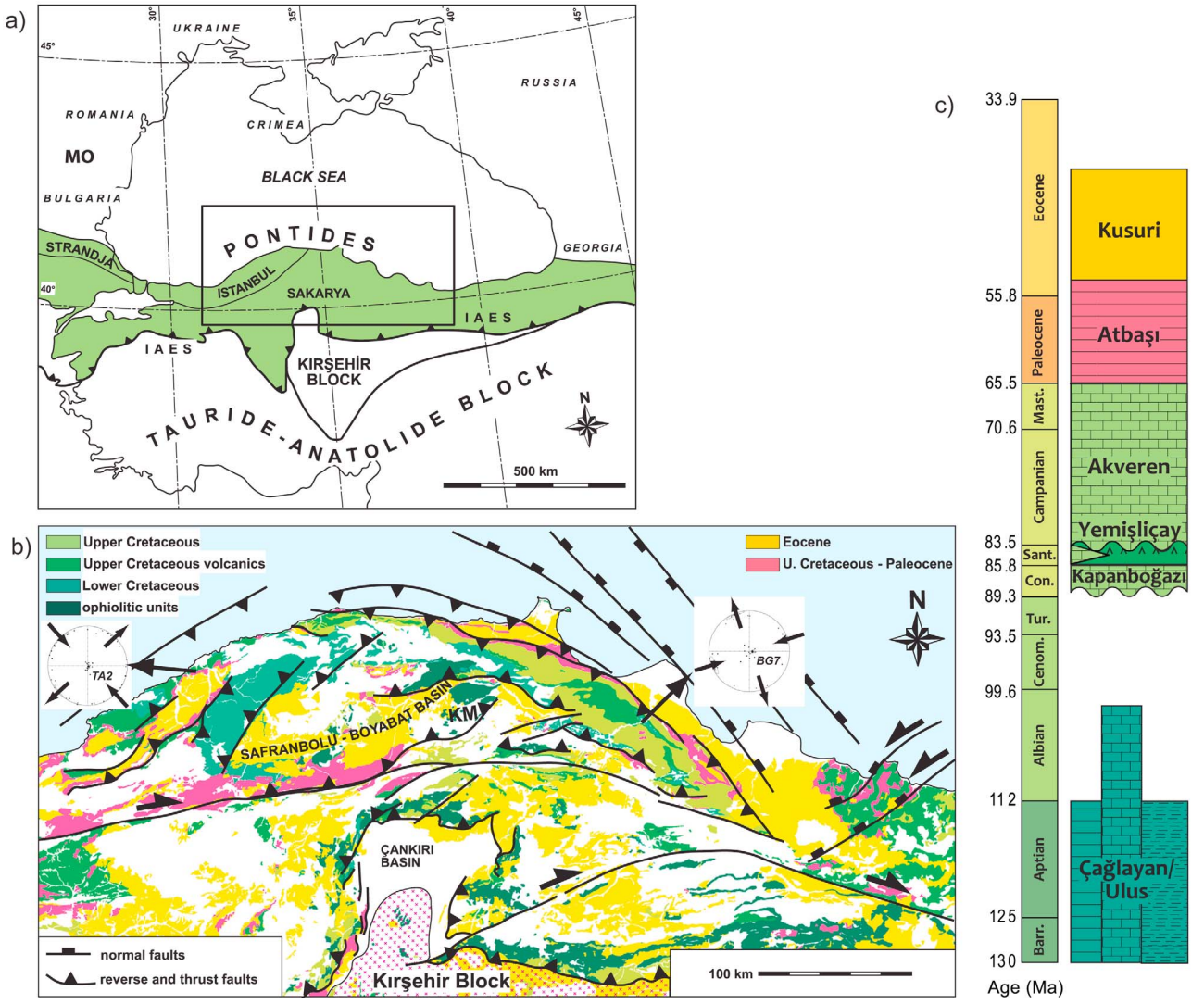


**Figure 1.** (a) Map showing the location of the Pontides in relation to the Black Sea, the Izmir-Ankara-Erzincan (IAE) suture, the Kırşehir Block and the Anatolide-Tauride Block. MO indicates the position of the Moesian Platform. (b) Zoom of the map in Figure 1a, showing the main stratigraphic ages and major structures and basins in the central Pontides. The trend of the faults/basins is roughly NE/SW in the western part of the convex geometry, and NW/SE in the eastern part. In the south the Çankırı Basin and the Kırşehir Block are displayed. The results of the AMS measurements of sites TA2 and BG7 (Figure 8) are also indicated. KM indicates the location of the Kargı Massif. (c) Stratigraphic column following *Hippolyte et al.* [2010] showing the main formations that were sampled in this study. In the Cenomanian-Turonian there is a depositional gap.

also examined paleolatitude data from two of our sites and corrected them for inclination error using the E/I method of *Tauxe and Kent* [2004] to assess the paleolatitude of the Pontides in the late Cretaceous with respect to the predicted paleolatitude of the southern Eurasian margin from the apparent polar wander (APW) path of Eurasia [*Torsvik et al.*, 2008].

## 2. Geological Setting

[5] The Pontides in northern Turkey are a late Cretaceous to Paleogene fold-and-thrust belt between the Black Sea in the north and the Izmir-Ankara-Erzincan (IAE) suture zone in the south (Figure 1a) [*Okay and Tüysüz*, 1999]. The IAE suture zone separates the Pontides from the continental Anatolide-Tauride platform, and marks the former position of the subduction zone of a branch of the Neo-Tethys ocean. The Pontides comprise, from west to east, the Strandja Zone, İstanbul Zone and Sakarya Zone (Figure 1a).

[6] The Variscan basement of the Strandja Zone is covered by Triassic-Jurassic sedimentary rocks and the Strandja Zone underwent a second phase of deformation and metamorphism during the latest Jurassic to earliest Cretaceous. [*Gerdjikov*, 2005; *Okay et al.*, 2001a].

[7] The Sakarya Zone is structurally the lowest of these zones and underthrusts the Strandja and İstanbul Zones [*Okay et al.*, 2001a]. Unlike the İstanbul Zone, it includes a strongly deformed Variscan basement and the locally metamorphosed pre-Jurassic Karakaya Complex, which is described either as a mid-late Triassic subduction-accretion complex, or as an inverted rift basin [e.g., *Genç and Yilmaz*, 1995; *Pickett and Robertson*, 2004; *Okay and Göncüoğlu*, 2004].

[8] The İstanbul Zone is structurally the highest zone and is separated from the Strandja Zone by a right-lateral strike-slip fault [*Okay et al.*, 2001a]. It comprises non-metamorphic Ordovician to Carboniferous sedimentary sequences that were deformed during the Permo-Carboniferous, and are overlain by Triassic sediments [*Okay et al.*, 1994]. Based on its stratigraphy it is assumed that it is a detached block of the Moesian Platform that displaced southward during the opening of the western Black Sea basin [*Okay et al.*, 1994] (Figure 1a).

[9] The Sakarya and İstanbul Zones share a post-mid Jurassic volcano-sedimentary cover, while the post-Triassic cover of Sakarya is composed of lower Jurassic continental to shallow marine clastic rocks, with several ammonitico-rosso levels [*Altıner et al.*, 1991] which is either lacking in the İstanbul zone or poorly developed. In the eastern part of the Sakarya Zone (in general called the eastern Pontides), the lower and middle Jurassic units comprise volcanic and volcanoclastic sequences [*Yılmaz and Kandemir*, 2006; *Yılmaz et al.*, 2003], which are largely missing in the central and western Pontides. Platform carbonates of the İnaltı Formation of mid-Jurassic (Callovian) to early Cretaceous age cover the entire Pontides, except for the Strandja Zone. The entire cover of the Pontides consists of Cenomanian-Maastrichtian volcano-sedimentary sequences collectively named as Yemişliçay Formation in Turkey and Srednogorie Zone in the Balkans [*Okay et al.*, 1994; *Sinclair et al.*, 1997; *Zimmerman et al.*, 2008]. The Paleozoic basement of the Pontides suggests a Eurasian origin [*Bozkurt et al.*, 2008; *Okay et al.*, 2008], as opposed to the Pan-African origin of the Anatolide-Tauride belt [*Hetzel and Reischmann*, 1996; *Kröner and Şengör*, 1990; *Satır and Friedrichsen*, 1986; *Şengör et al.*, 1988].

[10] The Pontides have been separated from Europe by the Black Sea since the early Cretaceous [*Görür*, 1988; *Hippolyte et al.*, 2010; *Okay et al.*, 1994; *Tüysüz*, 1999], which comprises two major (western and eastern) sub-basins. Opening of the western Black Sea basin is generally considered to be early middle Cretaceous (Barremian-Albian) in age [*Görür*, 1997; *Robinson et al.*, 1996]. Timing of opening of the eastern Black Sea is still controversial, because of poor exposure of its stratigraphy. Early Cretaceous [*Kriachtchevskaia et al.*, 2010; *Nikishin et al.*, 2003] to early Cenozoic ages [*Robinson et al.*, 1995a] and even Eocene ages [*Vincent et al.*, 2005] are proposed, mainly based on incompatible and independent data sets and geophysical, stratigraphical, structural and tectonic modeling studies. It is generally accepted that the Cretaceous to Tertiary units in the Pontides are related to the opening of the Black Sea basins. Therefore, precise dating of these units is crucial in terms of understanding the ages of these basins. In this study we followed the stratigraphic classification scheme of *Hippolyte et al.* [2010], which is the most up-to-date and precise classification, based on 165 nannoplankton ages (Figure 1c) belonging to every lithostratigraphical unit in the Pontides. The most important difference with respect to former studies [i.e., *Görür*, 1997; *Tüysüz*, 1999] is related to the stratigraphic positions and ages of the Kapanboğazı/Yemişliçay and Akveren formations. The Kapanboğazı/Yemişliçay formations are stratigraphically transitional and now ascribed to the Coniacian to Santonian. The Akveren Formation is now considered to be of Campanian to Maastrichtian age.

[11] The syn-rift deposits of *Görür* [1997] of the western Black Sea basin in the Pontides comprise the Hauterivian-Albian Cağlayan/Ulus Group [*Hippolyte et al.*, 2010]. The Cenomanian-Turonian interval is marked by a hiatus: deposition resumed during the Coniacian and gave way to the deposition of red pelagic limestones (Kapanboğazı Formation) that gradually pass upwards into volcanics and volcanoclastic turbidites (Yemişliçay Formation) of Coniacian-Santonian age [*Hippolyte et al.*, 2010]. In Campanian-Maastrichtian times the Akveren/Alaplı limestones and siliciclastic turbidites of the Gürsökü Formation were deposited. This sedimentation was followed by deposition of limestones and marls of the Atbaşı Formation in the Paleocene. The turbiditic Kusuri Formation was deposited during the Eocene along the present-day Black Sea coast [*Özcan et al.*, 2007; *Robinson et al.*, 1995b], as well as volcano-sedimentary units of Eocene age that were deposited along a narrow band along the IAE suture zone [*Keskin et al.*, 2008]. Nummulitic limestones were deposited further away from the Black Sea coast in shallow water basins, developing over compressional structures [*Kaymakci et al.*, 2009; *Özcan et al.*, 2007; *Robinson et al.*, 1995b].

[12] The continental Anatolide-Tauride Block is located south of the IAE suture zone. The promontory of the Anatolide-Tauride Block in the central part of the bend in the Pontides and IAE suture zone that forms the present study area is the metamorphosed Kırşehir Block [*Görür et al.*, 1984]. At the contact between the Pontides and the Anatolide-Tauride Block, the Çankırı Basin developed as a late Cretaceous forearc and Paleogene foreland basin, straddling the IAE suture zone at the northernmost tip of the Kırşehir Block (Figure 1b). Metamorphism of the Kırşehir Block followed northward intraoceanic subduction and southward ophiolite emplacement over the Kırşehir Block during the Cenomanian to Turonian [*Kaymakci et al.*, 2009; *Whitney et al.*, 2001; *Yalınız et al.*, 2000]. This was followed by late Cretaceous to Paleocene northward oceanic subduction below the Pontides, as evidenced by the development of an upper Cretaceous volcanic arc on the Pontides [*Kaymakci et al.*, 2009; *Okay et al.*, 2001b, 2006; *Rice et al.*, 2006; *Tüysüz and Tekin*, 2007] and the development of a forearc basin in the Çankırı region [*Kaymakci et al.*, 2009]. Exhumation of the Kırşehir Block started at the end of the Cretaceous [*Boztuğ and Jonckheere*, 2007; *Görür et al.*, 1984] and continued during the Paleogene [*Boztuğ et al.*, 2009a, 2009b; *Gautier et al.*, 2002; *Isik*, 2009]. This implies that the Kırşehir Block may have formed a rigid indenter in the Paleogene, between the Anatolide-Tauride Block and the Pontides, which led to the development of a foreland basin in the Çankırı region [*Kaymakci*, 2000; *Kaymakci et al.*, 2009].

[13] The Pontides were underthrusted during Cenomanian-Turonian times (~100–89 Ma) by the Kargı Massif (Figure 1b), which was interpreted by *Okay et al.* [2006] as a microcontinental sliver of Neo-Tethyan origin, north of the Anatolide-Tauride Block.

## 3. Paleomagnetic Sampling, Analysis, and Results

### 3.1. Paleomagnetic Sampling

[14] In total, 1301 cores from 47 sites were sampled in the central and eastern Pontides, in lower Cretaceous to Eocene deposits, with a minimum of 7 up to as much as 149 cores per site; a single core often provided multiple specimens for paleomagnetic analysis (see Table 1). Samples were collected using a gasoline powered motor drill or an electric drill with generator, depending on the rock type. Sample orientations were measured with a magnetic compass, and sample orientations as well as bedding tilt were corrected for present-day declination, ranging from 4 to 5°W. Ages were assigned to formations according to *Hippolyte et al.* [2010] and those for the trachyandesites of site BD4 according to *Eyüboğlu* [2010].

### 3.2. Paleomagnetic Analysis

[15] Out of 1301 cores, 1064 specimens were demagnetized. The samples were demagnetized using alternating field (AF) and thermal (TH) progressive stepwise demagnetization methods. Approximately half of the samples that were AF demagnetized were heated until 150°C before AF demagnetization to remove possible stress in magnetite grains caused by surface oxidation at low temperatures [*Van Velzen and Zijderveld*, 1995; see also *Gong et al.*, 2008]. The largest part of the samples was demagnetized by AF demagnetization, and TH demagnetization was applied to test reproducibility of the AF results.

[16] Orthogonal vector diagrams [*Zijderveld*, 1967] were used to display demagnetization of the NRM (Figure 2). Sample ChRM directions were determined using principal component analysis [*Kirschvink*, 1980] on approximately five to seven successive AF or temperature steps in the majority of the samples. Samples that yielded NRM directions that were intermediate between two overlapping coercivity or temperature components, were analyzed using the great circle approach [*McFadden and McElhinny*, 1988]. With this method, the direction that lies closest on the great circle to the average direction from well-determined NRM directions can be determined (e.g., TA5.10B, Figure 2). Usage of the great circle approach is indicated in Table 1 and Figure 3.

[17] The majority of the samples has a characteristic remanent magnetization (ChRM) carried by magnetite, as is evidenced by typical maximum unblocking temperatures below 600°C or maximum unblocking fields of 60–100 mT. Occasionally, lower temperatures are sufficient to determine the ChRM, typically in the range 360–480°C which suggests that the remanence is mainly carried by greigite [*Roberts*, 1995; *Rowan et al.*, 2009; *Vasiliev et al.*, 2008]. In a number of cases there is also clear evidence for (additional) hematite as a carrier of the NRM (see below).

[18] Examples of comparable results of AF and thermal demagnetization can be found in Figure 2 (EK19.A/EK.19B, K8.6/K8.11 and TA2.40A/TA2.137A). In the pink/red pelagic limestones of the Kapanboğazı Formation (sites TA2 and EK), the magnetic carrier is magnetite, because the samples reach the origin between ~570°C–600°C, enabling AF demagnetization (see Figure 2). Examples of rocks wherein the main magnetic carrier is hematite are sites BG5 and BG7 (Figure 2, BG5.72B and BG7.37A). Thermal demagnetization on these samples was carried out until 630°C to reach the origin. Therefore, AF demagnetization until 90 mT after heating until 150°C resulted in a relatively small decrease of the NRM (Figure 2, BG5.29A). Since both sites BG5 and BG7 and sites TA2 and EK were taken from the red pelagic limestones of the Kapanboğazı Formation, we conclude that the magnetic carrier within this formation ranges from magnetite to hematite dominated rocks.

[19] From the ChRM directions, site means as well as virtual geomagnetic poles (VGP) and their means were calculated. A variable cut-off [*Vandamme*, 1994] was applied on the VGPs per site and we calculated the error in declination ($\Delta$Dx) and the error in inclination ($\Delta$Ix) separately, following *Butler* [1992]. We favor this approach because it more realistically describes the directional distributions that become increasingly ellipsoidal (elongated) with lower latitudes [*Creer et al.*, 1959]. To determine whether two distributions share a common true mean direction (CTMD), we use the test developed by [*McFadden and McElhinny*, 1990] and their classification (A, B, C, indeterminate) based on the critical angle $g_c$ and the angle $g$ between the means. We use their test with simulation, which effectively is equivalent to using the *Watson* [1983] $V_w$ parameter. Sites K5 and K7 were combined, as they shared a CTMD (Table 1).

[20] Data from two sites were corrected for inclination shallowing in sediments, using the elongation/inclination (E/I) method of *Tauxe and Kent* [2004]. Since a large number of individual directions is required to apply the model (preferably N > 100), we only applied this method to our sites TA2 and TA5.

[21] On samples from sites TA2 and BG7, measurements to determine the anisotropy of magnetic susceptibility (AMS) were performed to determine the magnetic fabric of the sediments and to assess whether they have a mainly sedimentary or tectonic fabric. This may be indicative of the amount of strain the rocks underwent after deposition [*Hrouda*, 1982], since the maximum axis of the AMS tensor ($k_{max}$) will start aligning with the direction of maximum extension (i.e., perpendicular to the direction of maximum compression). Jelinek statistics [*Jelinek*, 1981, 1984] were used for these calculations.

### 3.3. Reliability Criteria

[22] The new data we present in this study, as well as previously published data, collected from Cretaceous, Paleocene and Eocene rocks, are obviously subject to many sources of error. Therefore we have chosen the following reliability criteria, applied to both our own and published data sets.

**Table 1.** Sampled Paleomagnetic Sites[a]

| | | | | | | | | | ChRM Directions (In Situ) | | | | | | | ChRM Directions (Tilt Corrected) | | | | | | | | VGPs (Tilt Corrected) | | | | |
|---|---|---|---|---|---|---|---|---|---|---|---|---|---|---|---|---|---|---|---|---|---|---|---|---|---|---|---|---|
| Site | Age | Formation | Rocktype | Lat | Lon | Nc | Pol | Gc | N/Na | D | ΔDx | I | ΔIx | k | α95 | N/Na | D | ΔDx | I | ΔIx | palat | k | α95 | λ | ϕ | K | A95 | Rej |
| **A1** | Barremian-Aptian | Çağlayan | shales | 41.7 | 32.4 | 14 | n | | 14/14 | 21.3 | 12.3 | 19.2 | 22.2 | 9.9 | 13.3 | 14/14 | 18.9 | 12.2 | 28.1 | 19.6 | **15.0** | 10.4 | 12.9 | 58.7 | 175.4 | 12.4 | 11.8 | |
| A2 | Barremian-Aptian | Çağlayan | shales | 41.7 | 32.4 | 14 | | | 15/15 | 66.5 | 34.5 | 61.0 | 21.2 | 5.8 | 17.4 | 15/15 | 228.5 | 99.9 | 86.9 | 15.1 | **83.8** | 5.8 | 17.4 | 37.5 | 26.6 | 2.6 | 29.9 | 4,6 |
| **A3** | Barremian-Aptian | Çağlayan | shales | 41.7 | 32.4 | 14 | n | | 7/14 | 45.1 | 11.5 | 31.9 | 17.3 | 27.9 | 11.6 | 7/14 | 33.1 | 18.7 | 53.6 | 15.9 | **34.1** | 27.9 | 11.6 | 63.0 | 127.7 | 16.3 | 15.4 | |
| **A4** | Coniacian-Santonian | Kapanboğazı | red pelagic limestones | 41.7 | 32.4 | 10 | r | Gc | 7/7 | 210.5 | 9.9 | -44.2 | 11.3 | 28.5 | 11.5 | 7/7 | 213.3 | 9.7 | -41.5 | 11.9 | **23.9** | 28.5 | 11.5 | 57.1 | 144.7 | 47.2 | 8.9 | |
| **ER** | Coniacian-Santonian | Yemişliçay | clays/ volcanoclastics | 41.3 | 31.5 | 16 | n | | 14/14 | 331.5 | 8.2 | 40.3 | 10.3 | 24.2 | 8.3 | 14/14 | 320.2 | 9.0 | 48.2 | 9.1 | **29.2** | 24.1 | 8.3 | 55.7 | -66.2 | 26.7 | 7.8 | |
| **EE** | Coniacian-Santonian | Kapanboğazı | red pelagic limestones | 41.3 | 31.5 | 15 | r | Gc | 12/13 | 169.2 | 6.4 | -44.6 | 7.3 | 56.7 | 5.8 | 12/13 | 170.0 | 5.9 | -39.7 | 7.5 | **22.5** | 56.7 | 5.8 | 69.4 | -121.3 | 65.1 | 5.4 | |
| **EK** | Coniacian-Santonian | Kapanboğazı | red pelagic limestones | 41.3 | 31.6 | 19 | n | Gc | 14/14 | 328.6 | 3.2 | 36.6 | 4.4 | 141.0 | 3.4 | 14/14 | 322.6 | 3.9 | 47.9 | 4.0 | **29.0** | 138.1 | 3.4 | 57.3 | -68.5 | 136.9 | 3.4 | |
| EZ | Barremian-Albian | Çağlayan | shales | 41.4 | 31.7 | 17 | n | | 10/14 | 3.8 | 11.7 | 61.0 | 7.4 | 54.3 | 6.6 | 10/14 | 275.1 | 16.7 | 57.7 | 12.1 | **38.4** | 16.9 | 10.7 | 27.6 | -30.1 | 11.1 | 13.1 | 4,5 |
| K1 | Campanian-Maastrichtian | Akveren | limestones | 41.6 | 34.4 | 12 | | | 13/14 | 346.6 | 18.5 | 70.9 | 6.9 | 41.6 | 6.5 | 13/14 | 354.0 | 7.4 | -43.4 | 8.7 | **25.3** | 41.4 | 6.5 | 22.9 | -139.7 | 39.1 | 6.7 | 4 |
| **K2** | Eocene | Kusuri | shales | 41.5 | 34.7 | 12 | n | | 14/14 | 354.9 | 6.3 | 41.0 | 7.8 | 41.2 | 6.3 | 14/14 | 1.7 | 8.7 | 53.6 | 7.4 | **34.1** | 41.2 | 6.3 | 82.5 | -156.2 | 31.6 | 7.2 | |
| **K3** | Barremian-Albian | Çağlayan | shales | 41.6 | 34.8 | 12 | r | Gc | 13/14 | 188 | 17.3 | 44.0 | 19.7 | 7.1 | 16.7 | 12/14 | 186.2 | 14.9 | -43.6 | 17.2 | **25.5** | 12.2 | 12.9 | 73.1 | -164.8 | 11.4 | 13.4 | |
| K4 | Coniacian-Santonian | Yemişliçay | flysch | 41.7 | 34.9 | 13 | | | 8/14 | 356.4 | 22.7 | 56.3 | 17.3 | 13.0 | 16.0 | 8/14 | 143.5 | 29.3 | 56.5 | 22.0 | **37.1** | 13.0 | 16.0 | -4.5 | 63.3 | 6.8 | 23.0 | 4,5 |
| K5 | Campanian-Maastrichtian | Akveren | sparitic limestones | 41.8 | 35.0 | 7 | r | Gc | 4/7 | 227.2 | 11.1 | -39.7 | 14.2 | 65.7 | 11.4 | 4/7 | 207.8 | 8.5 | -30.9 | 13.0 | **16.7** | 73.3 | 10.8 | | | 128.5 | 8.1 | K5_7 |
| K6 | Eocene | Kusuri | marls | 41.9 | 35.1 | 14 | n | | 10/14 | 18.3 | 12.0 | 47.0 | 12.7 | 17.9 | 11.7 | 10/14 | 358.1 | 99.9 | 86.8 | 9.9 | **83.6** | 18.0 | 11.7 | 48.3 | 34.8 | 7.0 | 19.7 | 4,6 |
| K7 | Campanian-Maastrichtian | Gürsökü/Akveren | marls | 41.7 | 35.2 | 12 | r | Gc | 7/14 | 206.6 | 10.9 | -3.1 | 21.7 | 30.8 | 11.0 | 7/14 | 207.0 | 16.8 | -33.9 | 24.4 | **18.6** | 41.4 | 14.5 | | | 34.2 | 15.9 | K5_7 |
| **K5_K7** | Campanian-Maastrichtian | Gürsökü/Akveren | limestones/marls | | | 19 | r | Gc | 11/21 | 212.9 | 11.1 | -16.6 | 20.7 | 11.4 | 14.1 | 11/21 | 208.3 | 7.7 | -30.2 | 12.0 | **16.2** | 41.5 | 7.2 | 54.7 | 163.1 | 39.2 | 7.4 | |
| **K8** | Paleocene | Atbaşı | marly/sandy limestones | 41.7 | 35.3 | 13 | n | | 10/14 | 8.9 | 37.0 | 71.0 | 13.2 | 13.6 | 13.6 | 10/14 | 355.3 | 11.6 | 32.0 | 17.5 | **17.4** | 13.6 | 13.6 | 65.3 | -133.9 | 19.9 | 11.1 | |
| **K9** | Coniacian-Santonian | Kapanboğazı | red pelagic limestones | 41.0 | 36.1 | 13 | n | | 9/14 | 31.3 | 2.9 | 6.0 | 5.7 | 326.0 | 4.6 | 11/14 | 36.8 | 11.8 | 42.9 | 13.9 | **24.9** | 12.1 | 13.7 | 55.5 | 142.4 | 19.3 | 10.7 | |
| **K10** | Coniacian-Santonian | Kapanboğazı | red pelagic limestones | 41.1 | 36.0 | 7 | n | | 13/13 | 77 | 2.2 | 37.4 | 3.0 | 324.6 | 2.3 | 13/13 | 55.9 | 2.7 | 43.0 | 3.2 | **25.0** | 324.4 | 2.3 | 41.4 | 127.2 | 284.4 | 2.5 | |
| D1 | Eocene | Kusuri | sands and silts | 41.4 | 32.0 | 15 | | | 0/7 | | | | | | | | | | | | | | | | | | | |
| **D2** | Eocene | Kusuri | mud/silt/sandstones | 41.3 | 32.0 | 12 | r | | 12/14 | 182.5 | 4.8 | 2.4 | 9.6 | 37.6 | 7.2 | 12/14 | 182.0 | 6.5 | -35.6 | 9.1 | **19.7** | 37.6 | 7.2 | 68.3 | -153.1 | 51.2 | 6.1 | |
| **D3** | Eocene | Kusuri | mudstones/marls | 41.3 | 32.0 | 13 | n | | 13/14 | 14.4 | 22.4 | 70.3 | 8.6 | 24.9 | 8.5 | 13/14 | 353.7 | 6.8 | 28.7 | 10.8 | **16.3** | 24.9 | 8.5 | 63.4 | -134.3 | 41.3 | 6.5 | |
| D4 | Campanian-Maastrichtian | Akveren | limestones | 41.2 | 32.2 | 15 | | | 8/14 | 318.1 | 28.6 | 52.8 | 24.7 | 10.6 | 17.8 | 8/14 | 304.8 | 14.8 | -3.2 | 29.6 | **-1.6** | 10.6 | 17.8 | 48.6 | -127.2 | 14.9 | 14.8 | 4 |
| **D5** | Paleocene | Atbaşı | red and green marls | 41.2 | 32.2 | 12 | n+r | Gc | 5/7 | 206.5 | 22.7 | -44.8 | 25.4 | 10.8 | 24.4 | 5/7 | 166.5 | 19.5 | -21.8 | 34.3 | **11.3** | 10.8 | 24.4 | 57.9 | -122.5 | 16.9 | 19.1 | |
| **F1** | Eocene | Kusuri | marls | 40.8 | 37.2 | 15 | r | Gc | 13/34 | 129.9 | 4.3 | -40.5 | 5.4 | 83.4 | 4.4 | 13/34 | 177.4 | 5.5 | -53.1 | 4.7 | **33.6** | 108.3 | 4.0 | 82.6 | -125.8 | 83.9 | 4.6 | |
| **F2** | Eocene | Kusuri | limestones | 40.9 | 37.3 | 13 | r | | 15/19 | 176.2 | 10.2 | -37.2 | 13.9 | 13.7 | 10.7 | 15/19 | 171.3 | 10.0 | -35.3 | 14.2 | **19.5** | 14.0 | 10.6 | 67.3 | -121.0 | 17.3 | 9.5 | |
| F3 | Paleocene | Atbaşı | clayey limestones | 40.9 | 37.3 | 15 | n | Gc | 24/27 | 3.4 | 3.5 | 38.8 | 4.6 | 80.3 | 3.3 | 23/27 | 3.6 | 6.2 | 62.8 | 3.6 | **44.2** | 94.3 | 3.1 | 85.8 | 74.8 | 48.0 | 4.4 | 6 |
| F4 | Paleocene | Atbaşı | silt/sand/mudrocks | 41.1 | 37.2 | 13 | n | Gc | 8/13 | 188.5 | 9.5 | -61.8 | 5.8 | 110.6 | 5.3 | 8/13 | 205.3 | 10.6 | -64.1 | 5.8 | **45.9** | 110.4 | 5.5 | 71.1 | 104.2 | 58.0 | 7.3 | 6 |
| F5 | Paleocene | Atbaşı | clayey limestones | 41.1 | 36.3 | 8 | | | 10/11 | 251.2 | 99.9 | -71.4 | 54.6 | 1.6 | 62.7 | 10/11 | 314.8 | 99.9 | -41.7 | 89.3 | **24.0** | 1.6 | 62.7 | 12.6 | -102.1 | 1.5 | 66.8 | 4 |
| KE1 | Maastrichtian | Akveren | oolitic limestones | 41.2 | 31.9 | 65 | | | 0/19 | | | | | | | | | | | | | | | | | | | |
| **KE2** | Eocene | ? | sandy mudstones | 41.2 | 31.5 | 41 | r | Gc | 28/47 | 175.7 | 5.8 | -12.3 | 11.1 | 19.1 | 6.4 | 27/47 | 181.5 | 6.4 | -30.8 | 9.8 | **16.6** | 22.2 | 6.0 | 65.4 | -152.0 | 21.8 | 6.1 | |
| **KE3** | Paleocene | Atbaşı | marls and limestones | 41.7 | 32.4 | 34 | n | | 38/54 | 355.2 | 3.9 | 41.3 | 4.8 | 37.8 | 3.8 | 38/54 | 9.1 | 5.5 | 52.3 | 4.9 | **32.9** | 34.6 | 4.0 | 78.6 | 170.1 | 26.5 | 4.6 | |
| **KE4** | Eocene | Kusuri | clays | 41.6 | 32.3 | 15 | n | | 9/12 | 349.4 | 15.2 | -0.2 | 30.4 | 9.1 | 18.1 | 9/12 | 350.7 | 16.4 | 18.1 | 30.0 | **9.3** | 9.1 | 18.1 | 56.7 | -130.8 | 11.1 | 16.2 | |
| **KE5** | middle Eocene | Kusuri | shaly marls | 41.6 | 32.4 | 51 | n | | 25/47 | 6.6 | 12.8 | 35.6 | 17.9 | 5.5 | 13.6 | 25/47 | 38.8 | 18.9 | 53.6 | 16.0 | **34.1** | 5.3 | 14.0 | 58.8 | 123.3 | 4.5 | 15.5 | |

**Table 1.** (continued)

| Site | Age | Formation | Rocktype | Lat | Lon | Nc | Pol | Gc | ChRM Directions (In Situ) | | | | | | | ChRM Directions (Tilt Corrected) | | | | | | | | VGPs (Tilt Corrected) | | | | Rej |
|---|---|---|---|---|---|---|---|---|---|---|---|---|---|---|---|---|---|---|---|---|---|---|---|---|---|---|---|---|
| | | | | | | | | | N/Na | D | ΔDx | I | ΔIx | k | α95 | N/Na | D | ΔDx | I | ΔIx | palat | k | α95 | λ | ϕ | K | A95 | |
| **KE6** | middle Eocene | Kusuri | nummulitic limestones | 41.2 | 32.7 | 31 | r | | 33/44 | 185.5 | 11.7 | -35.1 | 16.6 | 5.4 | 11.9 | 33/44 | 185.5 | 11.7 | -35.1 | 16.6 | **19.4** | 5.4 | 11.9 | 67.7 | -161.1 | 6.1 | 11.0 | |
| **KE7** | early Eocene | Hacıhalil | mudstones/shale | 41.2 | 32.6 | 48 | n | | 57/61 | 352.8 | 2.6 | 40.6 | 3.3 | 58.3 | 2.5 | 57/61 | 353.0 | 3.1 | 48.7 | 3.1 | **29.7** | 57.1 | 2.5 | 77.1 | -119.0 | 48.9 | 2.7 | |
| KE8 | early Eocene | Hacıhalil | arkosic sands | 41.4 | 33.8 | 48 | | | 0/19 | | | | | | | | | | | | | | | | | | | |
| **KE9** | Paleocene | Atbaşı | marly limestones | 41.9 | 34.6 | 21 | n | Gc | 18/32 | 12.5 | 5.5 | -20.4 | 9.8 | 33.0 | 6.1 | 18/32 | 7.0 | 8.4 | 52.3 | 7.4 | **32.9** | 33.0 | 6.1 | 79.4 | -179.3 | 25.3 | 7.0 | |
| **KE10** | Eocene | Kusurı | silty/sandy clays | 41.9 | 35.1 | 27 | n | | 14/22 | 29.5 | 6.1 | -18.6 | 11.1 | 28.4 | 7.6 | 13/22 | 31.1 | 5.4 | 15.9 | 10.1 | **8.1** | 40.6 | 6.6 | 46.5 | 167.1 | 61.2 | 5.3 | |
| KE11 | early Eocene | Kusurı | yellow sands | 41.4 | 35.1 | 10 | | | 8/8 | 353.6 | 12.4 | 52.8 | 10.8 | 40.6 | 8.8 | 8/8 | 354.2 | 7.3 | -9.2 | 14.3 | **4.6** | 40.7 | 8.8 | 43.7 | -136.9 | 58.8 | 7.3 | 4,5 |
| KE12 | middle Eocene | Kocaçay | nummulitic limestones | 41.5 | 34.7 | 19 | | | 6/6 | 350.2 | 11.2 | 63.8 | 6.2 | 154.9 | 5.4 | 6/6 | 191.8 | 4.0 | 15.3 | 7.5 | **7.8** | 154.6 | 4.0 | -39.5 | 19.5 | 285.9 | 4.0 | 4,5 |
| **TA2** | Coniacian-Santonian | Kapanboğazı | red pelagic limestones | 41.7 | 32.4 | 149 | n | | 85/124 | 336.5 | 2.4 | 42.2 | 2.9 | 47.2 | 2.3 | 86/124 | 325.3 | 2.6 | 48.8 | 2.6 | **29.7** | 53.4 | 2.1 | 59.7 | -69.6 | 47.0 | 2.3 | |
| **TA5** | Santonian | Yemişliçay | volcanoclastics | 41.7 | 32.4 | 68 | r | Gc | 115/121 | 186.4 | 1.9 | -46.1 | 2.1 | 64.5 | 1.7 | 115/121 | 169.6 | 1.4 | -43.9 | 1.6 | **25.7** | 112.1 | 1.2 | 71.8 | -116.2 | 113.6 | 1.2 | |
| BG1 | Barremian-Aptian | Inaltı | limestones | 40.4 | 39.7 | 61 | r | | 13/15 | 186.3 | 27.3 | -29.1 | 43.2 | 3.8 | 24.8 | 13/15 | 193.5 | 24.5 | -13.7 | 46.5 | **6.9** | 3.8 | 24.7 | 54.4 | -163.8 | 3.9 | 24.3 | 4 |
| BD4 | Campanian | | tuffites | 40.1 | 40.3 | 65 | | Gc | 14/15 | 33.2 | 11.5 | 66.6 | 5.5 | 63.2 | 5.0 | 14/15 | 127.6 | 5.2 | 40.0 | 6.6 | **22.8** | 63.3 | 5.0 | -10.4 | 88.3 | 69.6 | 4.8 | 4 |
| **BG5** | Coniacian-Santonian | Kapanboğazı | red pelagic limestones | 40.8 | 39.6 | 73 | r | HT | 17/17 | 187.0 | 6.1 | -55.8 | 4.8 | 102.5 | 3.5 | 17/17 | 218.4 | 3.4 | -30.4 | 5.2 | **16.3** | 105.0 | 3.0 | 48.9 | 154.6 | 156.9 | 2.9 | |
| BG6 | Campanian-Maastrichtian? | Akveren | limestones | 40.7 | 37.6 | 64 | | | 9/15 | 111.3 | 30.3 | -44.4 | 34.2 | 6.2 | 22.5 | 9/15 | 86.0 | 37.7 | -53.7 | 31.1 | **34.2** | 105.8 | 3.5 | -18.9 | 157.0 | 122.1 | 3.2 | 4 |
| **BG7** | Coniacian-Santonian | Kapanboğazı | red pelagic limestones | 41.1 | 35.9 | 37 | n | | 17/27 | 85.3 | 4.2 | 35.4 | 6.0 | 78.9 | 4.0 | 17/27 | 74.7 | 4.1 | 43.1 | 4.8 | **25.1** | 114.2 | 3.4 | 27.3 | 115.4 | 95.1 | 3.7 | |

[a]Sampled paleomagnetic sites. Site number bold: accepted site. Age of the sites according to *Hippolyte et al.* [2010], formation name, rock type, latitude (Lat) and longitude (Lon) of the site. Number of sampled cores (Nc), polarity of the ChRM directions (pol, tilt corrected), use of great circle analysis (if used, indicated with Gc) [*McFadden and McElhinny*, 1988]. Number of samples after application of a variable cut-off on the VGPs of the ChRM direction (N) [*Vandamme*, 1994], over the number of samples that were measured (Na). Declination (D), inclination (I) and declination (ΔDx) and inclination (ΔIx) errors determined from the A95 of the poles, with corresponding estimate of the precision parameter (k) and cone of confidence ($\alpha_{95}$) determined from the ChRM directions for in situ and tilt corrected data. Latitude ($\lambda$) and longitude ($\varphi$) with corresponding estimate of the precision parameter (K) and cone of confidence determined from the mean virtual geomagnetic pole (VGP). Rej: reason of rejection of site (see section 3.3 and caption Table 2) for reference.

[23] Data(sets) with the following characteristics were excluded from further analyses: (1) Data sets sampled close to/in a major fault zone, (2) samples from data sets that were demagnetized using bulk demagnetization, (3) data sets that do not have a minimum number ($N \geq 5$) of samples (sediments) or sites (magmatic rocks), (4) data sets with suspect directions (i.e., N/down or S/up directions) that may result from a (partial) overprint (e.g., K1, see Figure 2, specimen K1.7) or large measuring errors caused by very low NRM intensities (Figure 2, specimens D1.12, KE1.6 and KE 8.20), (5) data sets that carry a direction which in geographic coordinates are not distinguishable from the present-day geocentric axial dipole field direction, (6) data sets with an inclination that is lower than can reasonably be expected from flattening. The flattening factor (f) relates the ratio of the observed inclination to the inclination of the (applied) field [*King*, 1955]. In natural sediments the flattening factor may range between zero (fully flattened) and unity (no flattening). However, typical values of f are 0.4–0.6 in sediments, but can be as low as 0.3 in red beds [*Tauxe and Kent*, 1984]. For all data, we use a lower boundary cut-off of $f \geq 0.3$. Finally, we rejected two sites (F3, F4) with an inclination more than 10° higher than suggested by the APW path [*Torsvik et al.*, 2008].

[24] An overview of previous paleomagnetic studies on 29 sites/localities in Cretaceous, Paleocene and Eocene rocks in the Pontides, north of the North Anatolian Fault Zone (NAFZ) is listed in Table 2. Most studies were carried out on Cretaceous rocks (18 studies), and data from nine Eocene localities were published (9), especially from the eastern Pontides (Figure 4). Only one study on Paleocene rocks was published. One site from a study by *Van der Voo* [1968] was previously assigned a Cretaceous age, but the most recent Turkish geological map (1:500,000 scale) [*Şenel et al.*, 2001] assigns a lower-middle Cretaceous age to those rocks. Two other sites from the study by *Van der Voo* [1968] were also given a new age according to the geological map (Table 2). Overall, the study carried out by *Channell et al.* [1996] and data from several sites analyzed by *Sarıbudak* [1989] and *Kissel et al.* [2003] were included for further analysis. In Table 2 we have indicated which sites were excluded from further discussion as well as the reason for exclusion.

## 4. Paleomagnetic Results

[25] Examples of orthogonal vector diagrams [*Zijderveld*, 1967] and equal area projections of the ChRM directions of all sites are given in Figures 2 and 3. After critical analysis of all measured sites, we have excluded 15 out of the sampled 47 sites (~32%) from further analysis (Figures 5a–5d).

[26] On the basis of this study, combined with literature data, we define four distinct areas in the Pontides – the western limb, the central zone, the eastern limb, and the eastern Pontide area – that have distinct rotation patterns (Figure 5e). From the rotation patterns in upper Cretaceous rocks, we can conclude that these were rotated counter-clockwise (until ~40°) in the western limb and clockwise (until ~40°) in the eastern limb, whereas no or only local rotations were found in the central zone and eastern Pontides (Figures 5e and 5f). Rocks from the four accepted Paleocene sites contain no significant rotation in all four segments. Furthermore, none of the eight accepted Eocene sites show a significant rotation. This means that we can demonstrate little or no vertical axis rotations in the Paleocene and the Eocene in the northern parts of the Pontides.

[27] To allow comparison of the paleolatitudinal position from the Pontides with the APW path, we corrected two of our sample sets (sites TA2 and TA5) for inclination error with the E/I method [*Tauxe and Kent*, 2004] (Figure 6). Correction is allowed because of the high quality of the data sets and the large number of analyzed samples. Site TA2 was sampled in red pelagic limestones of Coniacian-Santonian age, while the turbiditic volcanoclastics of site TA5 have a Santonian age according to *Hippolyte et al.* [2010]. Because of the normal paleomagnetic signal in site TA2 and the reversed paleomagnetic signal of TA5, the latter must be younger and late Santonian in age, since the magnetization has to be post-Cretaceous Normal Superchron. The original paleolatitude for site TA2 is 29.7°N, and for TA5 it is 25.7°N. Correction for both sites is small. For TA2 the TK03 corrected paleolatitude is 40.2° > 31.3° > 29.2°N, for site TA5 this is 35.0° > 26.6° > 25.5°N, which is insignificant (within the 95% bootstrap errors) in both cases (Figure 6). Within error, these TK03.GAD corrected inclinations are not significantly different than the inclination expected from the APW path.

[28] In Figure 7, the paleolatitudes with their error (calculated from $\Delta I_x$) are displayed. Figure 7 (left) shows the data from the literature review, Figure 7 (right) shows the data from our study. We also show the expected paleolatitudes when a flattening factor (f = 0.3–0.9) is applied to sediments [*King*, 1955]. The data distribution clearly shows the effect of inclination shallowing in sediments: the majority of the data yield lower values than the expected values from the APW path.

[29] On samples of sites TA2 and BG7, AMS measurements were performed (Figure 8). The alignment of the maximum axis is parallel to the structural trend in the area (Figure 1b), and perpendicular to the declination measured in the samples (Figure 4). When back-rotating the anisotropy axes according to the paleomagnetic declination, the maximum axis (lineation) aligns in an east-west direction, implying EW extension or NS compression.

## 5. Discussion

[30] On the basis of this paleomagnetic study we show that the convex northward shape of the Pontides is reflected in declinations of upper Cretaceous rocks (~90–83 Ma, in one case in rocks of ~83–65 Ma (K5–7). The sampled Paleocene and Eocene rocks do not show significant variations across the region. Hence, we conclude that the Pontides is an oro-

**Figure 2.** Orthogonal vector diagrams [*Zijderveld*, 1967], showing characteristic demagnetization diagrams for all sampled sites. Solid (open) circles indicate the projection on the horizontal (vertical) plane. An equal area plot of a demagnetization diagram that was interpreted using great-circle analysis is shown for TA5.10B: dashed (solid) line denotes projection on lower (upper) hemisphere. af= alternating field demagnetization, th= thermal demagnetization, tc= tilt corrected.

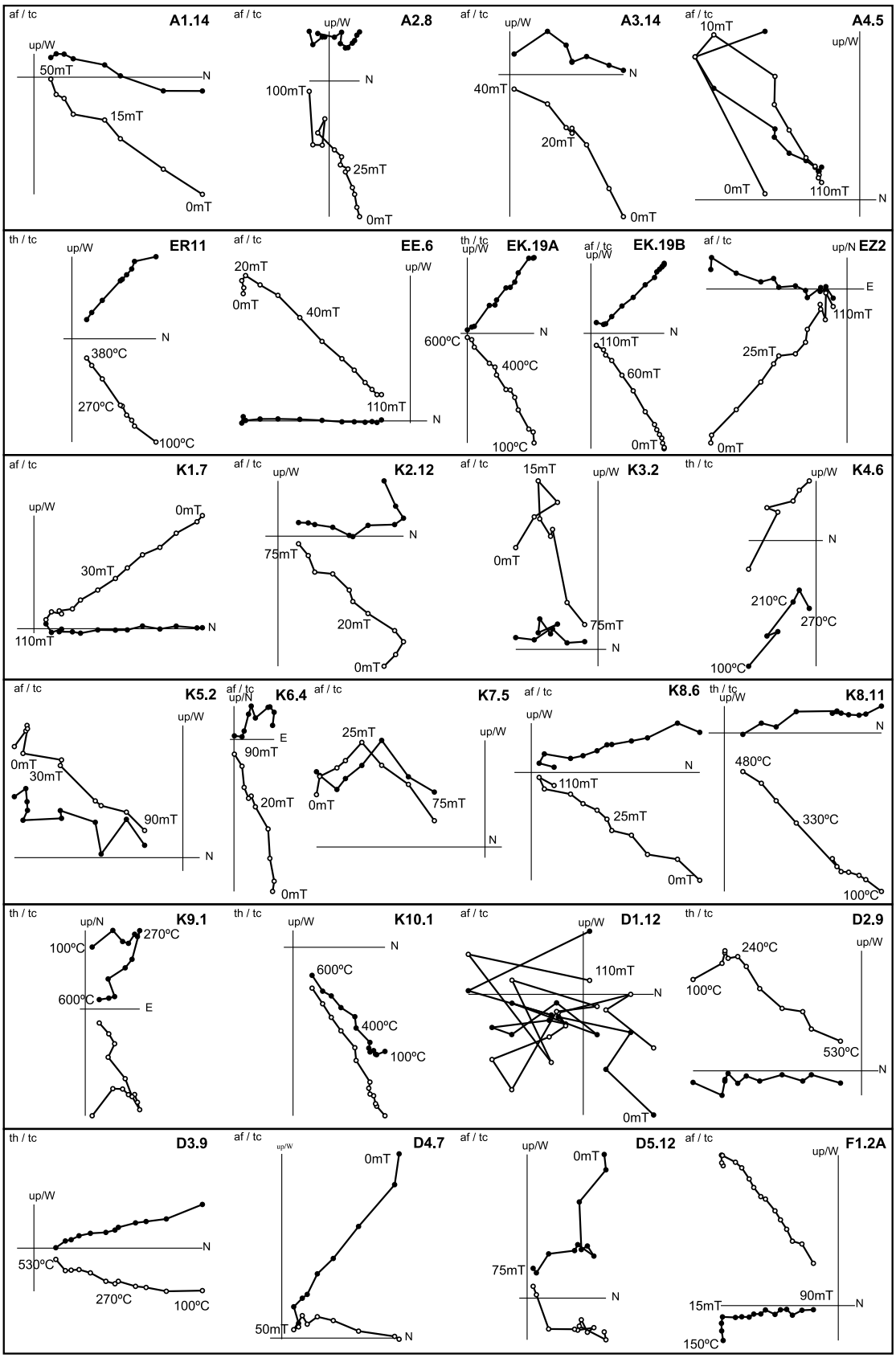
af / tc
A1.14
up/W
50mT
N
15mT
0mT
af / tc
A2.8
up/W
N
100mT
25mT
0mT
af / tc
A3.14
up/W
N
40mT
20mT
0mT
af / tc
A4.5
10mT
up/W
0mT
110mT
N
th / tc
ER11
up/W
N
380ºC
270ºC
100ºC
af / tc
EE.6
20mT
0mT
40mT
up/W
110mT
N
th / tc
EK.19A
up/W
N
600ºC
400ºC
100ºC
af / tc
EK.19B
up/W
N
110mT
60mT
0mT
af / tc
EZ2
up/N
E
110mT
25mT
0mT
af / tc
K1.7
up/W
0mT
30mT
110mT
N
af / tc
K2.12
up/W
N
75mT
20mT
0mT
af / tc
K3.2
15mT
up/W
0mT
75mT
N
th / tc
K4.6
up/W
N
210ºC
270ºC
100ºC
af / tc
K5.2
up/W
0mT
30mT
90mT
N
af / tc
K6.4
up/N
E
90mT
20mT
0mT
af / tc
K7.5
25mT
up/W
0mT
75mT
N
af / tc
K8.6
up/W
N
110mT
25mT
0mT
th / tc
K8.11
up/W
N
480ºC
330ºC
100ºC
th / tc
K9.1
up/N
270ºC
100ºC
600ºC
E
th / tc
K10.1
up/W
N
600ºC
400ºC
100ºC
af / tc
D1.12
up/W
110mT
N
0mT
th / tc
D2.9
240ºC
up/W
100ºC
530ºC
N
th / tc
D3.9
up/W
N
530ºC
270ºC
100ºC
af / tc
D4.7
up/W
0mT
50mT
N
af / tc
D5.12
up/W
0mT
75mT
N
af / tc
F1.2A
up/W
90mT
15mT
N
150ºC

**Figure 2**

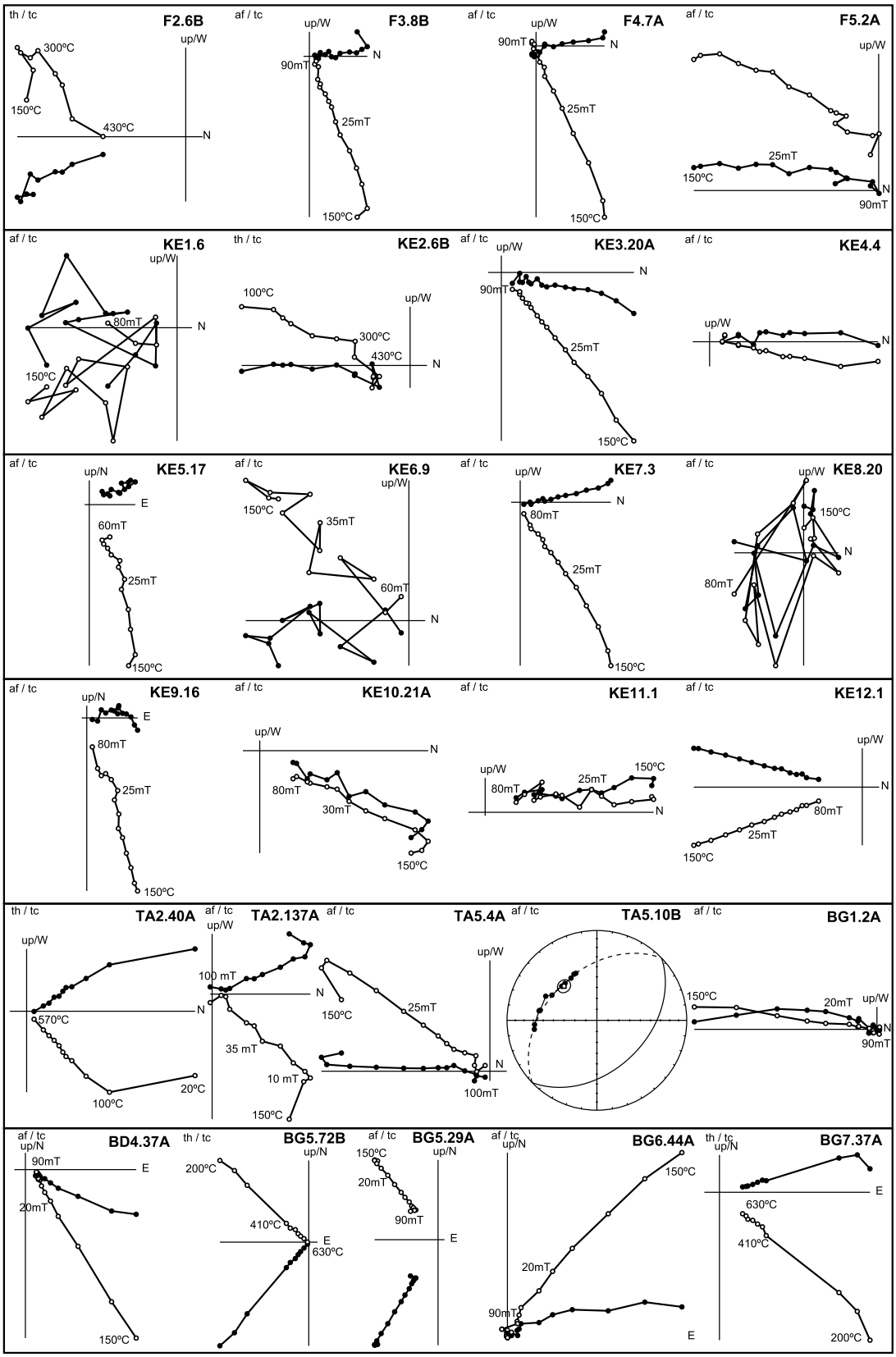


**Figure 2.** (continued)

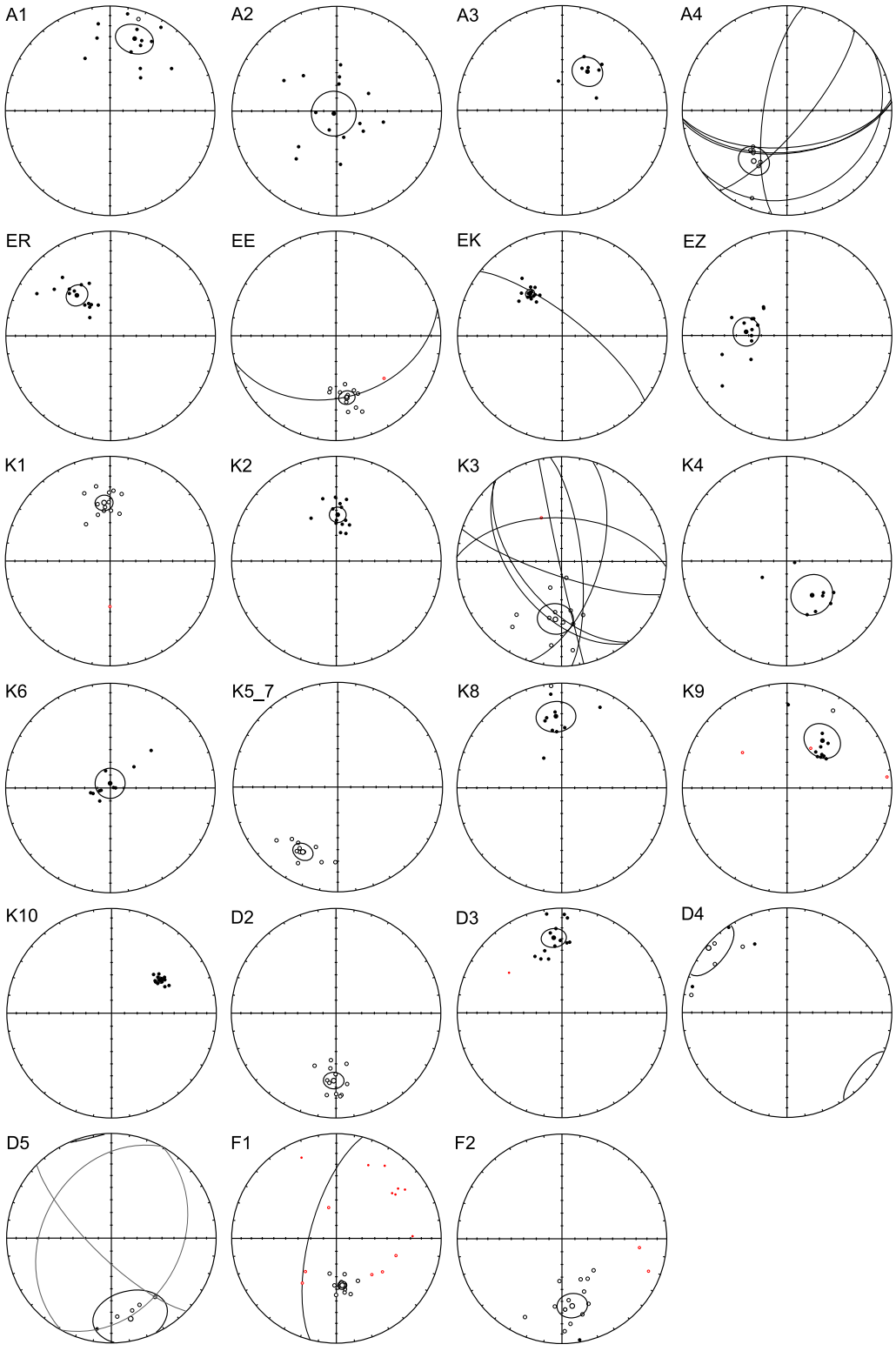


**Figure 3.** Equal area projections of the ChRM directions of all sites (Table 1). Open (solid) symbols denote projection on upper (lower) hemisphere. Large symbols indicate respectively the mean directions and their cone of confidence ($\alpha_{95}$). Red (small) circles indicate the individual directions rejected by the Vandamme cut-off angle [*Vandamme*, 1994]. Black lines indicate the great circles that were used to calculate the best fitting ChRM directions [*McFadden and McElhinny*, 1988].

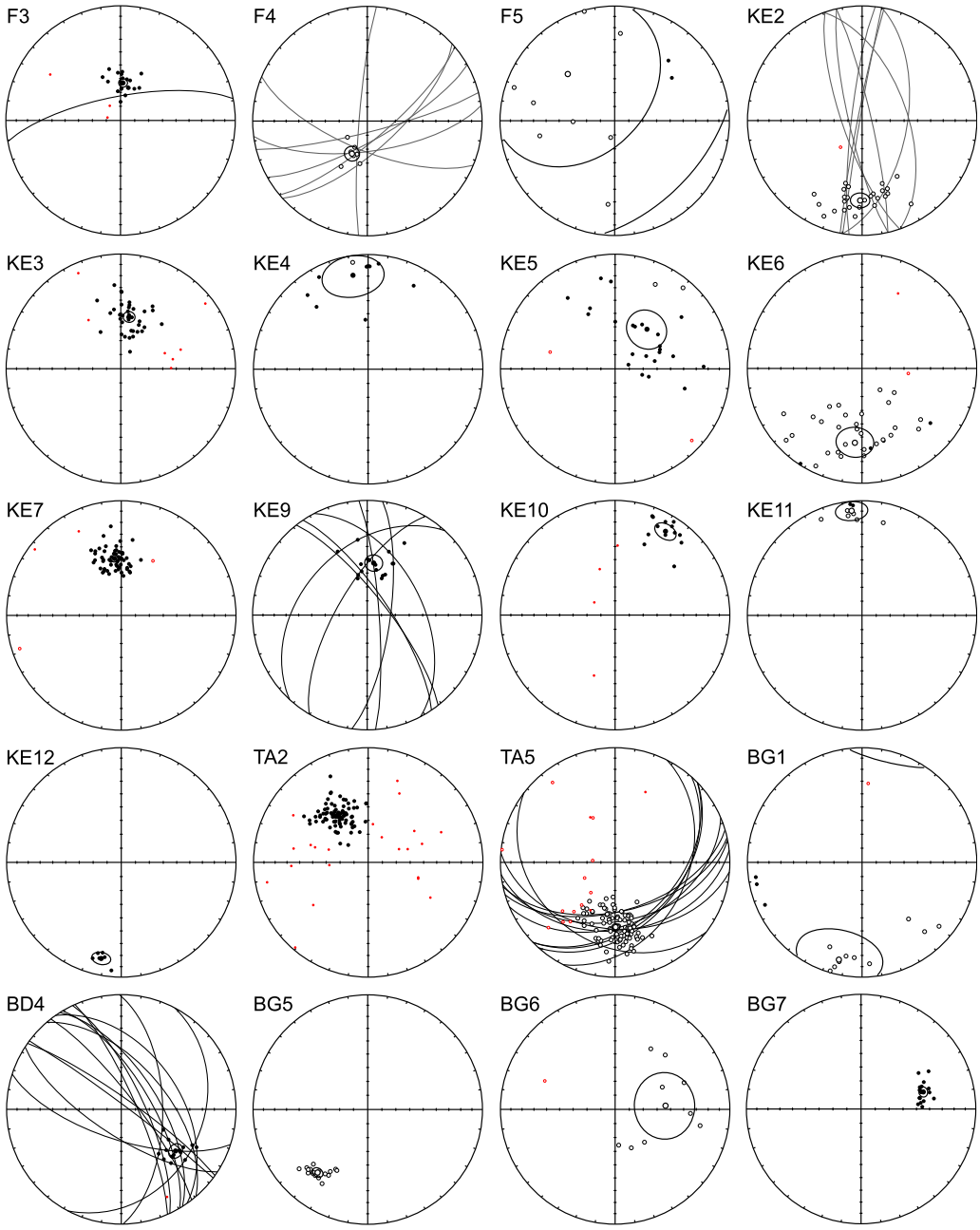


**Figure 3.** (continued)

cline that formed between latest Cretaceous (~83 Ma) and Paleocene (65 Ma). We suggest that the AMS directions are inherited from an early north-south compressional event and were rotated during orocline formation, because the magnetic lineations are nearly parallel when their present orientation is corrected for the paleomagnetically determined vertical-axis rotations at both sites. This is in contrast to the conclusions of *Scheepers and Langereis* [1994] who argued that the end phase of tectonic rotations (in the southern Apennines, Italy) probably corresponds to a blocking of the system. They concluded that the alignment of the magnetic lineation must have taken place (just) after tectonic rotations. On the contrary, in the Gran Sasso range (northern Apennines, Italy) *Sagnotti et al.* [1998] found magnetic lineations assuming a nearly parallel trend when their orientation is corrected for the vertical axis rotations. Moreover, their pattern of the magnetic lineation trends does not appear affected by recent extensional tectonics or by the development of late out-of-

sequence thrusts. Their observations strengthen our interpretation that the magnetic lineation in the sedimentary sequences of the central Pontides was induced at an early stage of tectonic deformation, during an early pre-rotational compressional phase. It seems that neither orocline formation or post-Cretaceous compression re-aligned the AMS directions (Figure 8).

[31] It is important to note that the magnitude of Coniacian to Campanian rotations is longitude-dependent (Figure 5f) and there is no rotation detected in the Paleocene units. This implies that the orocline formation in the Pontides took place approximately during the Maastrichtian to earliest Paleocene (70–65 Ma). However, *Kaymakci et al.* [2003] and *İşseven and Tüysüz* [2006] have reported that clockwise and counterclockwise rotations occurred during the Eocene-Oligocene interval in respectively the eastern and western side of the Çankırı Basin located to the south of the center of the orocline. In addition, there is general consensus that the convergence and related compressional deformation between the Anatolide-Tauride Block and the Pontides was continuous during the late Cretaceous to Eocene [*Kaymakci et al.*, 2003, 2009; *Okay et al.*, 1994; *Okay and Tüysüz*, 1999; *Robinson*, 1997; *Robinson et al.*, 1996; *Şengör and Yilmaz*, 1981; *Tüysüz*, 1999; *Tüysüz and Tekin*, 2007].

[32] The rocks from Eocene sites in the northern part of the Pontides contain no rotation while there are strong clockwise and counterclockwise rotations in the southern part of the Pontides, within the Çankırı Basin [*Kaymakci et al.*, 2003], and clockwise rotations east of the Çankırı Basin and IAE suture zone [*İşseven and Tüysüz*, 2006]. This implies southwards migration of the deformation front and shortening within the heart of the orocline between Maastrichtian to Oligocene. Deformation caused by ongoing convergence between Africa and Eurasia was more or less evenly distributed in the region while the shortening was taken up in the south along the Izmir-Ankara-Erzincan suture zone between the Maastrichtian and the Oligocene.

[33] The time constraints on orocline formation now allow us to assess which geodynamic processes may have caused it. There are several possible candidates that may explain oroclinal bending in the Pontides. These include (1) opening of the Black Sea basins, (2) collision of a continental sliver or seamount/oceanic plateau that was located south of the Eurasian margin within the Neo-Tethys Ocean and north of the Anatolide-Tauride Block, or (3) collision with the Anatolide-Tauride Block. Orocline formation in the Pontides occurred in latest Cretaceous-early Paleocene times and, therefore, timing of the above mentioned three options plays an important role.

[34] There are two main scenarios for the opening of the western Black Sea basin. According to *Görür* [1988] the opening of the western Black Sea basin is early Cretaceous (Albian to Cenomanian). According to *Tüysüz* [1999], however, the main opening of the western Black Sea basin took place later, during the Turonian to Maastrichtian interval. This discrepancy in timing is mainly caused by imprecise dating and the fact that a major unconformity between the lower and upper Cretaceous sequences was underestimated and regarded as a local event. The updated stratigraphy provided by *Hippolyte et al.* [2010] (Figure 1c) suggests that opening of the western Black Sea basin might have taken place in two different phases. The first phase took place from the Hauterivian to Albian while the main opening took place from the Coniacian to Santonian. These phases were separated by mid-Cretaceous (Albian to Turonian) uplift and erosion that lasted approximately 10 Myrs. Opening of the eastern Black Sea basin probably took place in a sense oblique to the margin of the (eastern) Pontides [*Robinson et al.*, 1996], and opening ages vary from early Cenozoic to Eocene [*Robinson et al.*, 1995a; *Shillington et al.*, 2008; *Vincent et al.*, 2005]. We conclude that the timing of opening of the Black Sea basins does not coincide with oroclinal bending, because rotation of the limbs certainly occurred after the pre-Santonian opening of the western Black Sea basin.

[35] The second possible candidate for orocline formation is the accretion of the Kargı microcontinent. Accretion of Kargı took place in Cenomanian-Turonian times [*Okay et al.*, 2006], which pre-dates oroclinal bending. The scale of the Kargı complex in comparison to the scale of the orocline (Figure 1b) also raises questions about the feasibility of this mechanism, and although collision might be responsible for the mid-Cretaceous unconformity in the central Pontides, the scale and the early timing of collision do not make this event a likely candidate to explain the orocline.

[36] The collision of the Pontides and the Anatolide-Tauride Block is the third possible mechanism. The metamorphosed promontory of the Anatolide-Tauride Block, the Kırşehir Block, is located just south of the hinge point of the Pontides orocline (Figure 1b). Part of the collisional history can be reconstructed from the Çankırı Basin that straddles the IAE suture zone. The evolution of the Çankırı Basin can be clearly subdivided into two phases: a late Cretaceous to middle Paleocene forearc evolution, and a late Paleocene-early Miocene foreland evolution phase [*Kaymakci et al.*, 2009]. The first phase marks a northward jump of subduction to the southern margin of the Pontides in the Santonian, leading to the deposition of arc volcanics and volcanoclastics of the Yemişliçay Formation [*Kaymakci et al.*, 2009; *Okay et al.*, 2001b]. This period coincides with extension in the Kırşehir Block [*Boztuğ et al.*, 2009b; *Gautier et al.*, 2008; *Isik*, 2009], that continued until the Maastrichtian and possibly early Paleocene. Although this may (partly) overlap with the formation of the orocline, a direct relationship between extension in the Kırşehir Block and oroclinal bending seems unlikely, since the Çankırı forearc basin suggests free subduction of the northern Neo-Tethys below the Pontides. By the late Paleocene the northern Neo-Tethys separating the Pontides and the Anatolide-Tauride Block was entirely consumed and collision between the Anatolide-Tauride Block and the Pontides occurred [*Okay et al.*, 2001b]. This was recorded by flysch deposition, unconformable on top of the CACC [*Kaymakci et al.*, 2009]. The age of collision of the Kırşehır Block and Anatolide-Tauride Block with the Pontides seems not to be in conflict with the proposed age of orocline formation, and therefore is the most plausible mechanism to explain the northward convex geometry of the Pontides.

[37] A study on the rotational history of the Çankırı Basin was performed by *Kaymakci et al.* [2003]. The formation of the striking omega shape of the Çankırı Basin was examined

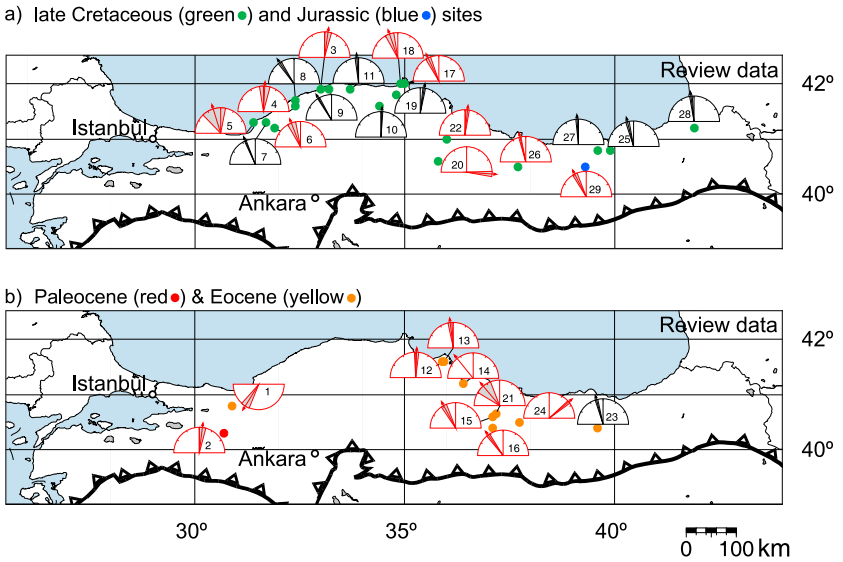


**Figure 4.** Paleomagnetic data from previous paleomagnetic studies. (a) Rotation vectors measured from Jurassic (in blue) and Cretaceous (in green) rocks of all previous paleomagnetic studies. (b) Rotation vectors measured from Paleocene (in red) and Eocene (in yellow) rocks of all previous paleomagnetic studies. $\Delta D_x$ envelopes of the rotation vectors shown in gray. Numbers correspond to the numbers in Table 2.

by performing paleomagnetic, AMS and paleostress measurements. Those data suggest that the omega shape of the Çankırı Basin was caused by ongoing indentation of the Kırşehir Block and Anatolide-Tauride Block until the Oligocene, not affecting the central Pontides orocline (Figure 9). Several paleomagnetic data sets from Eocene rocks in the study by *İşseven and Tüysüz* [2006] are in agreement with this scenario. The absence of studies on pre-Eocene rocks does not enable constraining initiation of rotation in the Çankırı Basin. Therefore, we cannot speculate on the possibility of simultaneous rotation in the Çankırı Basin and the Pontides orocline in the latest Cretaceous to earliest Paleocene times. However, the absence of rotation in the northern parts of the Pontides during the Paleocene to Oligocene in contrast with the presence of strong rotations in its southern parts may imply that the shortening and deformation front migrated southwards after the Paleocene (Figure 9). This scenario also implies that the Eocene-Oligocene rotations in the southern parts of the Pontides are related to thin-skinned thrusting within the suture zone.

[38] To assess the position of the Pontides in the late Cretaceous with respect to the Eurasian pole path, we corrected two of our sites for an inclination error, from which we have sufficient individual directions, using the E/I method of *Tauxe and Kent* [2004]. Figure 6 shows that inclination correction for Coniacian-Santonian site TA2 and Santonian site TA5 is limited to a few degrees. After correction for inclination error, the original inclination is within the 95% bootstrap error margin, meaning that the correction is not significant. Figure 7 shows that both sites plot 3 to 7 degrees in latitude lower than the expected paleolatitude from the Eurasian pole path (~34°N). We note however, that the A95 error envelope of the pole path (2–3°), overlaps with the error margins of the TK03 corrected values. Indeed, small differences of only a few degrees are close to the practical resolution limit (5°) of paleomagnetic studies.

[39] Nearly all reported paleolatitudes, from us as well as other authors, are lower than predicted by the APW path of *Torsvik et al.* [2008]. This may either represent inclination shallowing resulting from sediment compaction, or uncertainties in the APW path. The Eurasian APW path for the period after Pangea break-up is based on paleomagnetic data from all continents, rotated into Eurasian coordinates using rotation parameters derived from ocean floor anomalies and fracture zones. The paleomagnetic APW path is based on a rather limited and old data set, as in the last two decades most paleomagnetic research has focused on mobile belts rather than on stable continents. In recent years, several studies, especially from Asia, have shown paleolatitudinal discrepancies of up to ~10° between the APW path predictions and newly measured poles [*Cogné et al.*, 1999; *Dupont-Nivet et al.*, 2010; *Hankard et al.*, 2007a, 2007b], and have questioned the accuracy of the APW path. This debated APW resolution uncertainty may contribute to an explanation for our lower paleolatitudes. However, it is conceivable that inclination shallowing plays a significant role in the Pontides. The errors of many paleomagnetic localities from the Pontides are large enough to overlap with the APW path. Moreover, we showed above that the two sites that were successfully corrected for inclination shallowing, overlap within error with the APW path. Hence, at this stage it is not possible to make a conclusive distinction between the relative contribution of the two mechanisms, although we argue that using sediment-derived paleomagnetic data can in principle not be used to assess paleolatitude, unless tested and corrected for inclination shallowing. We calculated expected flattened latitudes from f-factors as low as 0.3 (Figure 7) that can explain the observed low paleolatitudes. Paleolatitudes were earlier assessed in a

**Table 2.** Paleomagnetic Data From Previous Studies[a]

| Site | Description | Lat | Lon | Age | Age Error | Dec | Inc | N/Ns | k | $\alpha_{95}$ | Study | Paleolatitude | Remarks | Reason of Exclusion |
|---|---|---|---|---|---|---|---|---|---|---|---|---|---|---|
| | | | | | | | *Western Limb* | | | | | | | |
| 1 | Eocene volcanics | 40.8 | 30.9 | 44.9 | 11.0 | 212.0 | 55.8 | 2m | 22.9 | 16.3 | *Sarıbudak et al.* [1990] | 36.3 | | 1 |
| 2 | Paleocene sediments | 40.3 | 30.7 | 60.7 | 4.9 | 187.3 | -30.1 | 33/3s | 15.9 | 32.0 | *Evans and Hall* [1990] | 16.2 | sites 10–13 | 1 |
| 3 | Yemişliçay Formation basalt | 41.9 | 33.0 | 86.4 | 2.9 | 188.3 | -27.0 | 6/1v | 69.0 | 8.1 | *Sarıbudak* [1989] | 14.3 | CI01 | 3 |
| 4 | Yemişliçay Formation andesite | 41.6 | 32.4 | 86.4 | 2.9 | 182.8 | -53.4 | 6/1v | 67.1 | 8.2 | *Sarıbudak* [1989] | 34.0 | BA01 | 3 |
| 5 | Yemişliçay Formation andesite | 41.3 | 31.4 | 86.4 | 2.9 | 163.3 | -56.7 | 5/1v | 20.0 | 17.5 | *Sarıbudak* [1989] | 37.3 | ER01 | 3 |
| 6 | Yemişliçay Formation andesite | 41.2 | 31.9 | 86.4 | 2.9 | 339.3 | 37.0 | 5/1m | 63.3 | 9.7 | *Sarıbudak* [1989] | 20.6 | DE01 | 3 |
| **7** | Yemişliçay Formation volcanoclastics | 41.3 | 31.7 | 86.4 | 2.9 | 336.8 | 41.3 | 59/5ms | 166.4 | 5.9 | *Channell et al.* [1996] | 23.7 | group 1 | |
| **8** | Yemişliçay/Kapanboğazı Formation | 41.7 | 32.4 | 86.4 | 2.9 | 325.7 | 45.4 | 47/3ms | 58.7 | 16.2 | *Channell et al.* [1996] | 26.9 | group 2 | |
| **9** | Yemişliçay/Kapanboğazı Formation | 41.9 | 33.2 | 86.4 | 2.9 | 329.1 | 41.6 | 116/9ms | 62.2 | 6.6 | *Channell et al.* [1996] | 23.9 | group 3 | |
| | | | | | | | *Central Zone* | | | | | | | |
| **10** | Yemişliçay Formation andesitic tuff | 41.6 | 34.4 | 86.4 | 2.9 | 1.9 | 29.4 | 23/1m | 243.0 | 4.3 | *Sarıbudak* [1989] | 15.7 | GÖ01–06 | |
| **11** | Yemişliçay/Kapanboğazı Formation | 41.9 | 33.7 | 86.4 | 2.9 | 356.0 | 40.3 | 71/6ms | 32.4 | 11.9 | *Channell et al.* [1996] | 23.0 | group 4 | |
| | | | | | | | *Eastern Limb* | | | | | | | |
| 12 | Eocene volcanics | 41.6 | 35.9 | 44.9 | 11.0 | 182.0 | -28.0 | 5/1m | 194.0 | 5.5 | *Sarıbudak* [1989] | 14.9 | BF01 | 3 |
| 13 | Eocene volcanics | 41.6 | 35.9 | 44.9 | 11.0 | 172.7 | -32.3 | 5/1m | 243.6 | 4.9 | *Sarıbudak* [1989] | 17.5 | BF02 | 3 |
| 14 | Eocene volcanics | 41.2 | 36.4 | 44.9 | 11.0 | 141.1 | -39.4 | 2/1m | N/A | N/A | *Sarıbudak* [1989] | 22.3 | SA01 | 3 |
| 15 | Eocene volcanics | 40.6 | 37.1 | 44.9 | 11.0 | 152.4 | -42.5 | 54/10m | 19.2 | 11.3 | *Tatar et al.* [1995] | 24.6 | north of NAFZ | 1 |
| 16 | Eocene volcanics | 40.4 | 37.0 | 44.9 | 11.0 | 144.1 | -47.5 | 63/8m | 54.0 | 7.6 | *Tatar et al.* [1995] | 26.8 | south of NAFZ | 1 |
| 17 | Yemişliçay Formation basalt | 42.0 | 35.0 | 86.4 | 2.9 | 154.9 | -39.0 | 6/1m | 157.2 | 5.3 | *Sarıbudak* [1989] | 22.0 | SI01 | 3 |
| 18 | Yemişliçay Formation basalt | 42.0 | 34.9 | 86.4 | 2.9 | 161.3 | -33.0 | 6/1m | 44.0 | 10.2 | *Sarıbudak* [1989] | 18.0 | SI02 | 3 |
| **19** | Yemişliçay/Kapanboğazı Formation | 41.8 | 34.8 | 86.4 | 2.9 | 9.1 | 40.2 | 63/5ms | 18.5 | 18.3 | *Channell et al.* [1996] | 22.9 | group 5 | |
| 20 | Vezirhan/Kapanboğazı Formation | 40.6 | 35.8 | 86.4 | 2.9 | 93.8 | 38.3 | 69/5ms | 5.3 | 36.7 | *Channell et al.* [1996] | 21.5 | group 6 | 1 |
| 21 | Middle-Upper Eocene volcanics[b] | 40.7 | 37.0 | 48.1 | 7.7 | 140.0 | -36.0 | 9/2m | 11.0 | 16.0 | *Van der Voo* [1968] | 20.0 | sites S-T | 3 |
| 22 | Çağlayan Formation andesites | 41.0 | 36.0 | 114.8 | 15.2 | 186.3 | 3.2 | 5/1m | 190.0 | 5.6 | *Sarıbudak* [1989] | 1.6 | KA01 | 3,6 |
| | | | | | | | *Eastern Pontides* | | | | | | | |
| **23** | Eocene limestones and volcanics | 40.4 | 39.6 | 44.9 | 11.0 | 345.0 | 35.0 | 82/9ms | 68.0 | 6.2 | *Kissel et al.* [2003] | 19.3 | Gümüşhane | |
| 24 | Eocene tuffs and dykes | 40.5 | 37.7 | 44.9 | 11.0 | 50.3 | 34.4 | 52/2m | 31.4 | 17.7 | *Orbay and Bayburdi* [1979] | 18.9 | O3–O4 | 2 |
| **25** | Upper Cretaceous limestones and volcanics[c] | 40.8 | 39.9 | 77.4 | 11.9 | 346.0 | 40.0 | 23/6ms | 90.0 | 7.0 | *Van der Voo* [1968] | 22.8 | sites F-L | |
| 26 | Upper Cretaceous tuffs and dykes | 40.5 | 37.7 | 77.4 | 11.9 | 346.8 | 49.9 | 241/7m | 30.6 | 9.6 | *Orbay and Bayburdi* [1979] | 30.7 | G1–G5, O1–O2 | 2 |
| **27** | Kapanboğazı Formation | 40.8 | 39.6 | 86.4 | 2.9 | 357.2 | 44.2 | 73/6s | 36.2 | 11.3 | *Channell et al.* [1996] | 25.9 | group 8/9 | |
| **28** | Kapanboğazı Formation | 41.2 | 41.9 | 86.4 | 2.9 | 353.1 | 43.2 | 129/10s | 35.0 | 8.3 | *Channell et al.* [1996] | 25.2 | group 10 | |
| 29 | Lower-Middle Jurassic sediments and volcanics[b,d] | 40.5 | 39.3 | 180.4 | 19.2 | 153.5 | -36.5 | 31/6ms | 35.0 | 11.0 | *Van der Voo* [1968] | 20.3 | sites M-R | |

[a]Sites numbers correspond to the numbers in Figure 4 and Figure 5. Site number bold: accepted site. Description of the sampled site (age and formation sampled). Site latitude (Lat), site longitude (Lon), age (assigned according to [*Luterbacher et al.*, 2004; *Ogg*, 2004; *Ogg et al.*, 2004]), declination (Dec), inclination (Inc), number of samples (N) from number of sites (Ns) from magmatic rocks (m), sedimentary rocks (s) or a combination of both (ms). Estimate of the precision parameter (k) and cone of confidence ($\alpha_{95}$) determined from ChRM directions. Cited study and calculated paleolatitude from ChRM directions. Remarks refer to site name in the cited study. Reason of exclusion of the site (if excluded), according to criteria mentioned in section 3.3.

[b]Cretaceous age rather than the age in the mentioned publication.

[c]Upper Cretaceous-Eocene age rather than the age in the mentioned publication.

[d]Has a newly assigned age that is too old for this study.

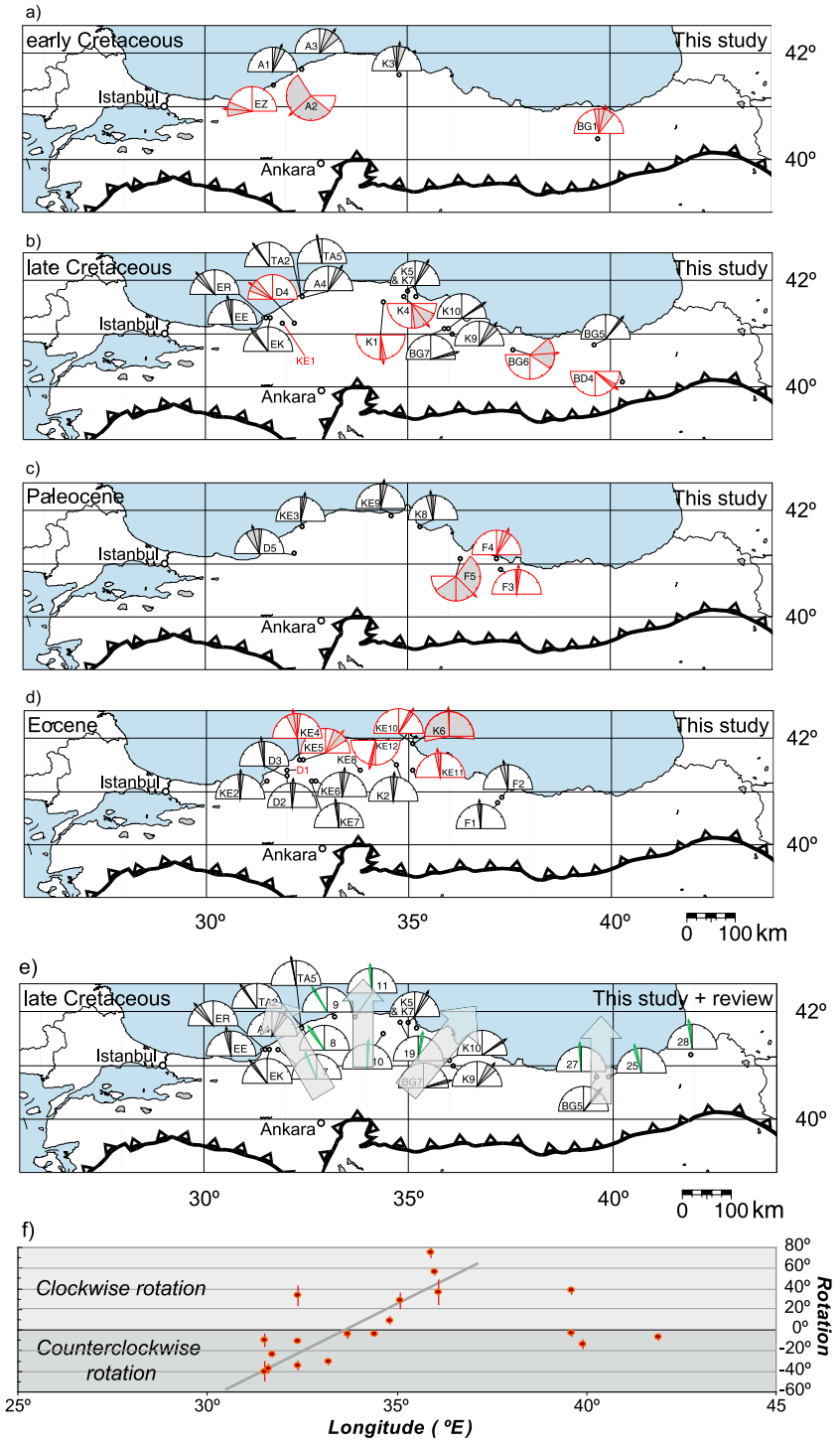


**Figure 5.** Paleomagnetic data from our study. $\Delta D_x$ errors of the rotation vectors are shown in gray. Numbers correspond to those in Table 2. Diagrams shown in red indicate rejected sites. Rotations measured from (a) early Cretaceous rocks, (b) late Cretaceous rocks, (c) Paleocene rocks and (d) Eocene rocks. (e) Map showing a compilation of all data from our study and from literature data from late Cretaceous rocks that pass our quality criteria. (f) Longitude versus rotation (declination) plot with all accepted data sets included. A clear trend from CCW rotation to zero rotation to CW rotation can be observed in the central Pontides.

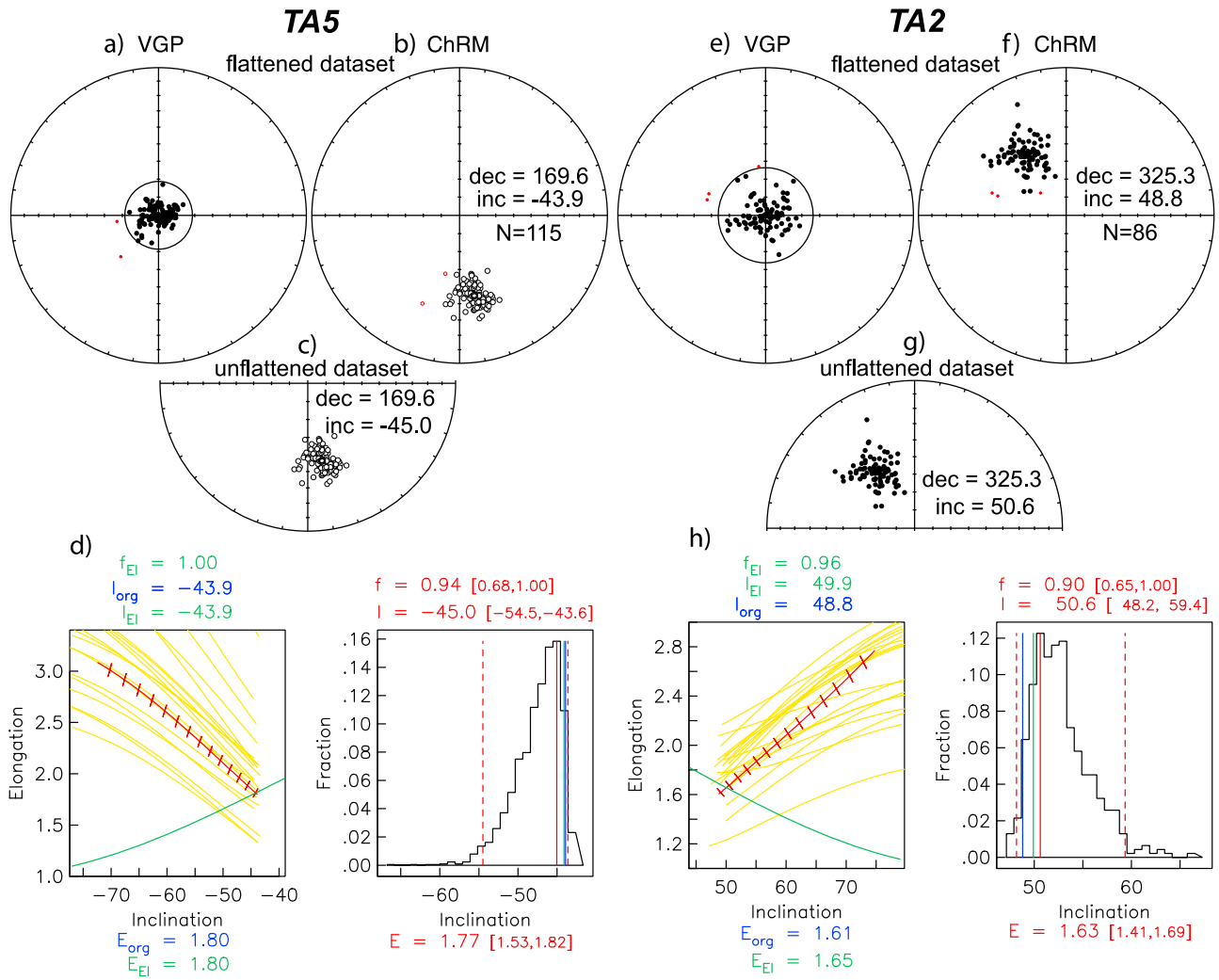


**Figure 6.** Equal-area projections of the individual VGP directions (a and e) before E/I correction and equal-area projections of the individual ChRM directions (b and f) before and (c and g) after E/I correction (symbols as in Figure 5) [*Tauxe and Kent*, 2004] with (d and h) corresponding (left) elongation versus inclination and (right) fraction (of 5000 bootstraps) versus inclination plots for TA5 (Figures 6a–6d) and TA2 (Figures 6e–6h). In Figure 6d and 6h (left) the E/I for the TK03.GAD model (green line) and for the data sets (red barbed line) for different degrees of flattening are plotted. The red barbs indicate the direction of elongation (horizontal is E–W and vertical is N–S). Also shown are examples (yellow lines) from 20 (out of 5000) bootstrapped data sets. The crossing points (if the data set intersects the model) represent the inclination/elongation pair most consistent with the TK03.GAD model, given as $inc_{EI}$ (in green) at the top; $inc_{org}$ = original inclination, $E_{org}$ = original elongation of the data set, $E_{EI}$ and $inc_{EI}$ are the elongation and inclination, respectively. In Figures 6d and 6h (right), a histogram of intersecting points from 5000 bootstrapped data sets is shown. The most frequent inclination (solid red vertical line; dashed red vertical lines denote the 95% bootstrap error) is given as value (and error range) on top; the inclinations of the original distribution (blue vertical line) or the intersection with the model (green vertical line) are indicated; E = the elongation resulting from the bootstrapped data sets.

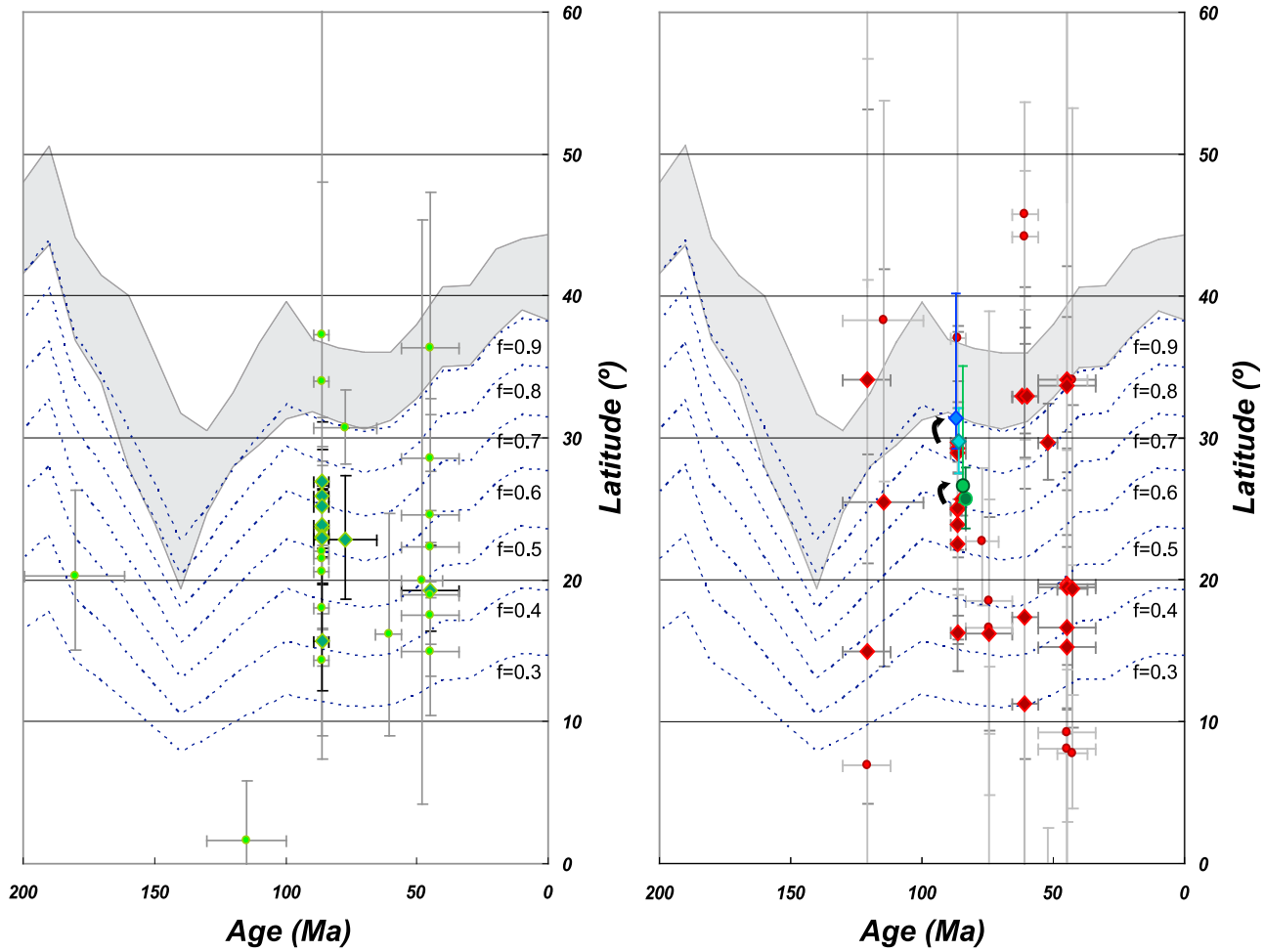


**Figure 7.** Paleolatitude versus age diagrams showing the expected paleolatitude for Eurasia with its $\Delta\lambda$ error envelope (in gray) calculated from the $\Delta I_x$ according to *Torsvik et al.* [2008]. Blue dotted lines show latitude versus age curve when a flattening of 0.9–0.3 was applied to the values calculated by the APW path [*King*, 1955]. (left) Large green diamonds (accepted) and small green circles (rejected) indicate paleolatitude with the $\Delta\lambda$ calculated from the $\Delta I_x$ that was obtained from A95 using the Creer transformation [*Creer*, 1962] on $\alpha_{95}$, usually given in literature (Table 2). (right) Large red diamonds (accepted) and small red circles (rejected) indicate paleolatitude with the $\Delta\lambda$ calculated from the $\Delta I_x$ (using A95) from this study. Blue diamonds (green circles) showing the paleolatitude of site TA2 (TA5) before and after correction with the E/I method of *Tauxe and Kent* [2004] with their error bars ($\Delta\lambda$ calculated from the $\Delta I_x$ for uncorrected data sets, 95% bootstrap error range for the TK03.GAD corrected data sets).

study by *Channell et al.* [1996], suggesting a gap in the APW path between Eurasia and Pontides of approximately 10° in paleolatitude (Figure 7), when compared to the pole path of *Torsvik et al.* [2008]. However, those data were all taken from sediments and not corrected for inclination error. Correction for inclination error on those data would probably result in a smaller gap between the Eurasian APW path and the location of the Pontides.

## 6. Conclusions

[40] Analysis of a large number (47 sites, more than 1000 cores) of paleomagnetic data, supplemented with published data, from rocks ranging in age from early Cretaceous to Eocene reveals that the northward convex shape of the central Pontides fold-and-thrust belt can be defined as an orocline that formed in latest Cretaceous to earliest Paleocene times. Orocline formation requires a deformation event such that the pre-existing structures are bent.

[41] Collision and indentation of the Anatolide-Tauride Block and its metamorphic promontory, the CACC, with the Pontides in late Paleocene times seems to be the most likely mechanism for orocline formation, considering the timing of oroclinal bending and the timing of collision between the Kırşehir Block and the Anatolide-Tauride Block with the Pontides. Paleomagnetic data from Eocene to Miocene rocks from the more southward located Çankırı Basin [*İşseven and*

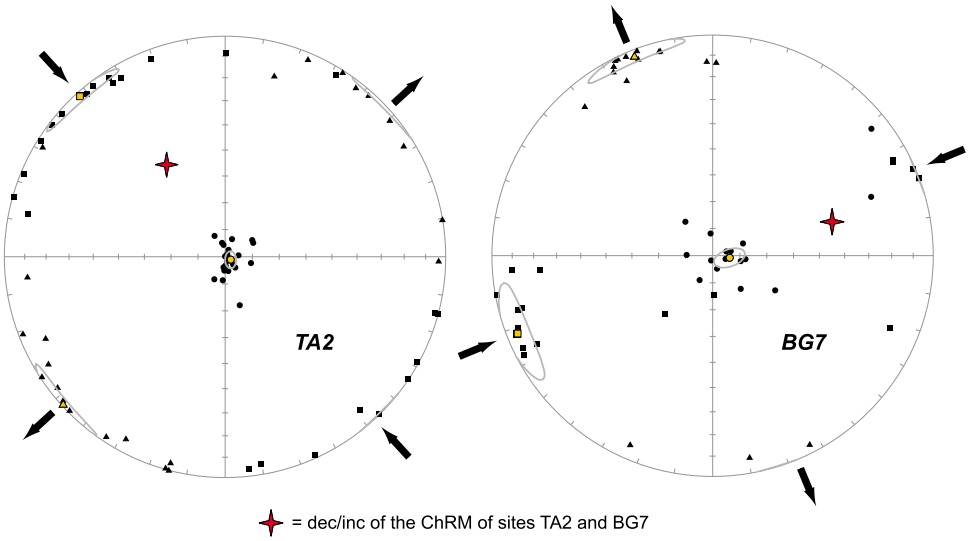


**Figure 8.** Equal-area projections of the AMS (anisotropy of the magnetic susceptibility) for sites (left) TA2 and (right) BG7. Yellow, large symbols indicate the mean of the tensor mean axes ($k_{min}$, $k_{int}$, $k_{max}$) and their error ellipses [*Jelinek*, 1981]. Arrows represent inferred extension/compression directions. Red star indicates the ChRM direction of the rocks from sites TA2 and BG7.

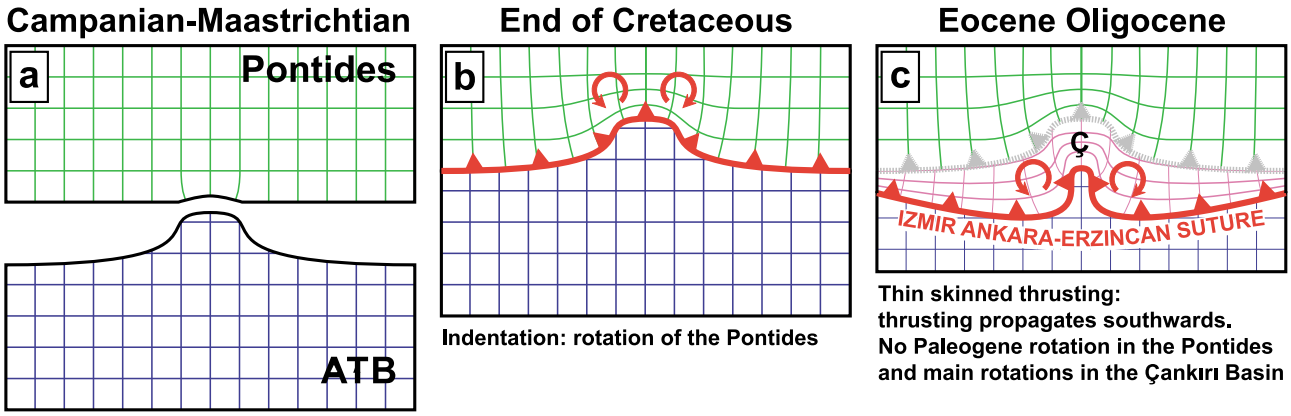


**Figure 9.** Conceptual model explaining the rotational history of the central Pontide orocline and the Çankırı Basin. (a) Campanian-Maastrichtian: Anatolide-Tauride Block (ATB) approaches the Pontides, (b) latest Cretaceous: collision of ATB with the Pontides causes orocline formation in the central Pontides, and (c) Eocene-Oligocene: thin-skinned thrusting propagates southwards, rotation in the central Pontides stops and concentrates in the Çankırı Basin.

*Tüysüz*, 2006; *Kaymakci et al.*, 2003], show strong rotations from Eocene to Oligocene times in this area, suggesting that the shortening and deformation front migrated southward.

[42] Furthermore, the majority of the paleolatitude data from the sampled sites and literature data show a (much) lower paleolatitude than predicted by the Eurasian APW path. Inclination error correction with the E/I-method of two of our sites that allow correction (N = ~100), predicts paleolatitudes that are within error identical to the Eurasian APW path. This, once more, shows that paleolatitude data from sediments should be interpreted with care.

[43] **Acknowledgments.** The authors would like to thank Bora Rojay and Yener Eyüboğlu for their help in the field to find suitable outcrops for sampling. Pınar Ertepınar, Ane Wiersma and Mustafa Kaya are also thanked for their help in the field. We thank two anonymous reviewers for their comments and suggestions. This work was financially supported by the Netherlands Research Centre for Integrated Solid Earth Sciences (ISES) and the Netherlands Organization for Scientific Research (NWO).

## References

Altıner, D., A. Koçyiğit, A. Farinacci, U. Nicosia, and M. A. Conti (1991), Jurassic-lower Cretaceous stratigraphy and paleogeographic evolution of the southern part of north-western Anatolia (Turkey), *Geol. Rom.*, *27*, 13–80.

Bozkurt, E., J. A. Winchester, E. Yiğitbaş, and C. J. Ottley (2008), Proterozoic ophiolites and mafic-ultramafic complexes marginal to the İstanbul Block: An exotic terrane of Avalonian affinity in NW Turkey, *Tectonophysics*, *461*, 240–251, doi:10.1016/j.tecto.2008.04.027.

Boztuğ, D., and R. C. Jonckheere (2007), Apatite fission track data from central Anatolian granitoids (Turkey): Constraints on Neo-Tethyan closure, *Tectonics*, *26*, TC3011, doi:10.1029/2006TC001988.

Boztuğ, D., Ö. Güney, M. Heizler, R. C. Jonckheere, M. Tichomirowa, and N. Otlu (2009a), 207Pb-206Pb, 40Ar-39Ar and fission-track geothermochronology quantifying cooling and exhumation history of the Kaman-Kırşehir region intrusions, central Anatolia, Turkey, *Turk. J. Earth Sci.*, *18*, 85–108.

Boztuğ, D., R. C. Jonckheere, M. Heizler, L. Ratschbacher, Y. Harlavan, and M. Tichomirova (2009b), Timing of post-obduction granitoids from intrusion through cooling to exhumation in central Anatolia, Turkey, *Tectonophysics*, *473*, 223–233, doi:10.1016/j.tecto.2008.05.035.

Butler, R. F. (1992), *Paleomagnetism: Magnetic Domains to Geologic Terranes*, 238 pp., Blackwell Sci., Boston.

Carey, S. W. (1958), The tectonic approach to continental drift, in *Continental Drift—A Symposium*, edited by S. W. Carey, pp. 177–363, Univ. of Tasmania, Hobart, Tasmania, Australia.

Channell, J. E. T., O. Tüysüz, O. Bektaş, and A. M. C. Şengör (1996), Jurassic-Cretaceous paleomagnetism and paleogeography of the Pontides (Turkey), *Tectonics*, *15*, 201–212, doi:10.1029/95TC02290.

Cogné, J.-P., N. Halim, Y. Chen, and V. Courtillot (1999), Resolving the problem of shallow magnetizations of Tertiary age in Asia: Insights from paleomagnetic data from the Qiangtang, Kunlun, and Qaidam Blocks (Tibet, China), and a new hypothesis, *J. Geophys. Res.*, *104*, 17,715–17,734.

Creer, K. M. (1962), The dispersion of the geomagnetic field due to secular variation and its determination for remote times from paleomagnetic data, *J. Geophys. Res.*, *67*, 3461–3476, doi:10.1029/JZ067i009p03461.

Creer, K. M., E. Irving, and A. E. M. Nairn (1959), Paleomagnetism of the Great Whin Sill, *Geophys. J. R. Astron. Soc.*, *2*, 306–323.

Dupont-Nivet, G., D. J. J. van Hinsbergen, and T. H. Torsvik (2010), Persistently low Asian paleolatitudes: Implications for the Indo-Asia collision history, *Tectonics*, doi:10.1029/2009TC002437, in press.

Evans, I., and S. A. Hall (1990), Paleomagnetic constraints on the tectonic evolution of the Sakarya Continent, northwestern Anatolia, *Tectonophysics*, *182*, 357–372, doi:10.1016/0040-1951(90)90172-5.

Eyüboğlu, Y. (2010), Late Cretaceous high-K volcanism in the eastern Pontide orogenic belt: Implications for the geodynamic evolution of NE Turkey, *Int. Geol. Rev.*, *52*, 142–186, doi:10.1080/00206810902757164.

Gautier, P., E. Bozkurt, E. Hallot, and K. Dirik (2002), Dating the exhumation of a metamorphic dome: Geological evidence for pre-Eocene unroofing of the Niğde Massif (central Anatolia, Turkey), *Geol. Mag.*, *139*, 559–576, doi:10.1017/S0016756802006751.

Gautier, P., E. Bozkurt, V. Bosse, E. Hallot, and K. Dirik (2008), Coeval extensional and lateral underflow during Late Cretaceous core complex development in the Niğde Massif, central Anatolia, Turkey, *Tectonics*, *27*, TC1003, doi:10.1029/2006TC002089.

Genç, S. C., and Y. Yilmaz (1995), Evolution of the Triassic continental margin, northwest Anatolia, *Tectonophysics*, *243*, 193–207, doi:10.1016/0040-1951(94)00198-I.

Gerdjikov, I. (2005), Alpine metamorphism and granitoid magmatism in the Strandja Zone: New data from the Sakar unit, SE Bulgaria, *Turk. J. Earth Sci.*, *14*, 167–183.

Gong, Z., C. G. Langereis, and T. A. T. Mullender (2008), The rotation of Iberia during the Aptian and the opening of the Bay of Biscay, *Earth Planet. Sci. Lett.*, *273*, 80–93, doi:10.1016/j.epsl.2008.06.016.

Görür, N. (1988), Timing of opening of the Black Sea Basin, *Tectonophysics*, *147*, 247–262, doi:10.1016/0040-1951(88)90189-8.

Görür, N. (1997), Cretaceous syn- to postrift sedimentation on the southern continental margin of the western Black Sea Basin, in *Regional and Petroleum Geology of the Black Sea and Surrounding Region*, edited by A. G. Robinson, pp. 227–240, Am. Assoc. of Pet. Geol., Tulsa, Okla.

Görür, N., F. Y. Oktay, İ. Seymen, and A. M. C. Şengör (1984), Paleotectonic evolution of the Tuzgölü Basin Complex, central Turkey: Sedimentary record of a Neo-Tethyan closure, in *The Geological Evolution of the Eastern Mediterranean*, edited by J. E. Dixon and A. H. F. Robertson, pp. 467–482, Geol. Soc. of London, London.

Hankard, F., J.-P. Cogné, V. Kravchinksy, L. Carporzen, A. Bayasgalan, and P. Lkhagvadorj (2007a), New Tertiary paleomagnetic poles from Mongolia and Siberia at 40, 30, 20, and 13 Ma: Clues on the inclination shallowing problem in central Asia, *J. Geophys. Res.*, *112*, B02101, doi:10.1029/2006JB004488.

Hankard, F., J. P. Cogné, X. Quidelleur, A. Bayasgalan, and P. Lkhagvadorj (2007b), Paleomagnetism and K-Ar dating of Cretaceous basalts from Mongolia, *Geophys. J. Int.*, *169*, 898–908, doi:10.1111/j.1365-246X.2007.03292.x.

Hetzel, R., and T. Reischmann (1996), Intrusion age of Pan-African augen gneisses in the southern Menderes Massif and the age of cooling after Alpine ductile extensional deformation, *Geol. Mag.*, *133*, 565–572, doi:10.1017/S0016756800007846.

Hippolyte, J.-C., C. Müller, N. Kaymakci, and E. Sangu (2010), Nannoplankton dating in the Black Sea inverted margin of central Pontides (Turkey) reveals two episodes of rifting, in *Sedimentary Basin Tectonics From the Black Sea and Caucasus to the Arabian Platform*, *Geol. Soc. London Spec. Publ. Ser.*, vol. 340, edited by M. Sosson et al., pp. 113–136, Geol. Soc. of London, London.

Hrouda, F. (1982), Magnetic anisotropy of rocks and its application in geology and geophysics, *Surv. Geophys.*, *5*, 37–82, doi:10.1007/BF01450244.

Isik, V. (2009), The ductile shear zone in granitoid of the Central Anatolian Crystalline Complex, Turkey: Implications for the origins of the Tuzgölü Basin during the Late Cretaceous extensional deformation, *J. Asian Earth Sci.*, *34*, 507–521, doi:10.1016/j.jseaes.2008.08.005.

İşseven, T., and O. Tüysüz (2006), Palaeomagnetically defined rotations of fault-bounded continental blocks in the North Anatolian Shear Zone, north central Anatolia, *J. Asian Earth Sci.*, *28*, 469–479, doi:10.1016/j.jseaes.2005.11.012.

Jelinek, V. (1981), Characterization of the magnetic fabric of rocks, *Tectonophysics*, *79*, T63–T67, doi:10.1016/0040-1951(81)90110-4.

Jelinek, V. (1984), On a mixed quadratic invariant of the magnetic-susceptibility tensor, *Z. Geophys.*, *56*, 58–60.

Kaymakci, N. (2000), Tectono-stratigraphical evolution of the Çankırı Basin (central Anatolia, Turkey), *Geol. Ultraiectina*, *190*, 1–247.

Kaymakci, N., C. E. Duermeijer, C. Langereis, S. H. White, and P. M. Van Dijk (2003), Palaeomagnetic evolution of the Cankiri Basin (central Anatolia, Turkey): Implications for oroclinal bending due to indentation, *Geol. Mag.*, *140*, 343–355, doi:10.1017/S001675680300757X.

Kaymakci, N., Y. Özçelik, S. H. White, and P. M. Van Dijk (2009), Tectono-stratigraphy of the Çankırı Basin: Late Cretaceous to early Miocene evolution of the Neotethyan suture zone in Turkey, in *Collision and Collapse at the Africa-Arabia-Eurasia Subduction Zone*, edited by D. J. J. Van Hinsbergen, M. A. Edwards, and R. Govers, pp. 67–106, Geol. Soc. of London, London.

Keskin, M., Ş. C. Genç, and O. Tüysüz (2008), Petrology and geochemistry of post-collisional Middle Eocene volcanic units in north-central Turkey: Evidence for magma generation by slab breakoff following the closure of the northern Neotethys Ocean, *Lithos*, *104*, 267–305, doi:10.1016/j.lithos.2007.12.011.

King, R. F. (1955), The remanent magnetism of artificially deposited sediments, *Geophys. J. Int.*, *7*, 115–134, doi:10.1111/j.1365-246X.1955.tb06558.x.

Kirschvink, J. L. (1980), The least squares line and plane and the analysis of paleomagnetic data, *Geophys. J. R. Astron. Soc.*, *62*, 699–718.

Kissel, C., C. Laj, A. Poisson, and N. Görür (2003), Paleomagnetic reconstruction of the Cenozoic evolution of the eastern Mediterranean, *Tectonophysics*, *362*, 199–217, doi:10.1016/S0040-1951(02)00638-8.

Kriachtchevskaia, O., S. Stovba, and R. Stephenson (2010), Cretaceous-Neogene tectonic evolution of the northern margin of the Black Sea from seismic reflection data and tectonic subsidence analysis, in *Sedimentary Basin Tectonics From the Black Sea and Caucasus to the Arabian Platform*, *Geol. Soc. London Spec. Publ. Ser.*, vol. 340, edited by M. Sosson et al., pp. 137–157, Geol. Soc. of London, London.

Kröner, A., and A. M. C. Şengör (1990), Archean and Proterozoic ancestry in late Precambrian to early Paleozoic crustal elements of southern Turkey as revealed by single-zircon dating, *Geology*, *18*, 1186–1190, doi:10.1130/0091-7613(1990)018<1186:AAPAIL>2.3.CO;2.

Luterbacher, H. P., et al. (2004), The Paleogene period, in *A Geologic Time Scale 2004*, edited by F. M. Gradstein, J. G. Ogg, and A. G. Smith, pp. 384–408, Cambridge Univ. Press, Cambridge, U. K.

McFadden, P. L., and M. W. McElhinny (1988), The combined analysis of remagnetization circles and direct observations in palaeomagnetism, *Earth Planet. Sci. Lett.*, *87*, 161–172, doi:10.1016/0012-821X(88)90072-6.

McFadden, P. L., and M. W. McElhinny (1990), Classification of the reversal test in palaeomagnetism, *Geophys. J. Int.*, *103*, 725–729, doi:10.1111/j.1365-246X.1990.tb05683.x.

Nikishin, A. M., M. V. Korotaev, A. V. Ershov, and M.-F. Brunet (2003), The Black Sea Basin: Tectonic history and Neogene-Quaternary rapid subsidence modelling, *Sediment. Geol.*, *156*, 149–168, doi:10.1016/S0037-0738(02)00286-5.

Ogg, J. G. (2004), The Jurassic period, in *A Geologic Time Scale 2004*, edited by F. M. Gradstein, J. G. Ogg, and A. G. Smith, pp. 307–343, Cambridge Univ. Press, Cambridge, U. K.

Ogg, J. G., F. P. Agterberg, and F. M. Gradstein (2004), The Cretaceous period, in *A Geologic Time Scale 2004*, edited by F. M. Gradstein, J. G. Ogg, and A. G. Smith, pp. 344–383, Cambridge Univ. Press, Cambridge, U. K.

Okay, A. I., and C. Göncüoğlu (2004), The Karakaya complex: A review of data and concepts, *Turk. J. Earth Sci.*, *13*, 77–95.

Okay, A. I., and O. Tüysüz (1999), Tethyan sutures of northern Turkey, in *The Mediterranean Basins: Tertiary Extension Within the Alpine Orogen*, edited by B. Durand et al., pp. 475–515, Geol. Soc. of London, London.

Okay, A. I., A. M. C. Şengör, and N. Görür (1994), Kinematic history of the opening of the Black Sea and its effect on the surrounding regions, *Geology*, *22*, 267–270, doi:10.1130/0091-7613(1994)022<0267:KHOTOO>2.3.CO;2.

Okay, A. I., M. Satır, O. Tüysüz, S. Akyüz, and F. Chen (2001a), The tectonics of the Strandja Massif: Late-Variscan and mid-Mesozoic deformation and metamorphism in the northern Aegean, *Int. J. Earth Sci.*, *90*, 217–233, doi:10.1007/s005310000104.

Okay, A. I., I. Tansel, and O. Tüysüz (2001b), Obduction, subduction and collision as reflected in the Upper Cretaceous-Lower Eocene sedimentary record of western Turkey, *Geol. Mag.*, *138*, 117–142, doi:10.1017/S0016756801005088.

Okay, A. I., O. Tüysüz, M. Satır, S. Özkan-Altıner, D. Altıner, S. Sherlock, and R. H. Eren (2006), Cretaceous and Triassic subduction-accretion, HP/LT metamorphism and continental growth in the central Pontides, Turkey, *Geol. Soc. Am. Bull.*, *118*, 1247–1269, doi:10.1130/B25938.1.

Okay, A. I., E. Bozkurt, M. Satır, E. Yiğitbaş, Q. G. Crowley, and C. K. Shang (2008), Defining the southern margin of Avalonia in the Pontides: Geochronological data from the Late Proterozoic and Ordovician granitoids from NW Turkey, *Tectonophysics*, *461*, 252–264, doi:10.1016/j.tecto.2008.02.004.

Orbay, N., and A. Bayburdi (1979), Palaeomagnetism of dykes and tuffs from the Mesudiye region and rotation of Turkey, *Geophys. J. R. Astron. Soc.*, *59*, 437–444.

Özcan, E., G. Less, and B. Kertész (2007), Late Ypresian to Middle Lutetian orthophragminid record from central and northern Turkey: Taxonomy and remarks on zonal scheme, *Turk. J. Earth Sci.*, *16*, 281–318.

Pickett, E., and A. H. F. Robertson (2004), Significance of the volcanogenic Nilufer Unit and related components of the Triassic Karakaya Complex for Tethyan subduction/accretion processes in NW Turkey, *Turk. J. Earth Sci.*, *13*, 97–143.

Rice, S. P., A. H. F. Robertson, and T. Ustaömer (2006), Late-Cretaceous- Early Cenozoic tectonic evolution of the Eurasian active margin in the central and eastern Pontides, northern Turkey, in *Tectonic Development of the Eastern Mediterranean Region*, edited by A. H. F. Robertson and D. Mountrakis, pp. 413–445, Geol. Soc. of London, London.

Roberts, A. P. (1995), Magnetic properties of sedimentary greigite (Fe3S4), *Earth Planet. Sci. Lett.*, *134*, 227–236, doi:10.1016/0012-821X(95)00131-U.

Robinson, A. G. (1997), Introduction: Tectonic elements of the Black Sea region, *AAPG Mem.*, *68*, 1–6.

Robinson, A., G. Spadini, S. Cloetingh, and J. Rudat (1995a), Stratigraphic evolution of the Black Sea: Inferences from basin modelling, *Mar. Pet. Geol.*, *12*, 821–835, doi:10.1016/0264-8172(95)98850-5.

Robinson, A. G., C. J. Banks, M. M. Rutherford, and J. P. P. Hirst (1995b), Stratigraphic and structural development of the eastern Pontides, Turkey, *J. Geol. Soc.*, *152*, 861–872, doi:10.1144/gsjgs.152.5.0861.

Robinson, A. G., J. H. Rudat, C. J. Banks, and L. F. Wiles (1996), Petroleum geology of the Black Sea, *Mar. Pet. Geol.*, *13*, 195–223, doi:10.1016/0264-8172(95)00042-9.

Rowan, C. J., A. P. Roberts, and T. Broadbent (2009), Reductive diagenesis, magnetite dissolution, greigite growth and paleomagnetic smoothing in marine sediments: A new view, *Earth Planet. Sci. Lett.*, *277*, 223–235, doi:10.1016/j.epsl.2008.10.016.

Sagnotti, L., F. Speranza, A. Winkler, M. Mattei, and R. Funiciello (1998), Magnetic fabric of clay sediments from the external northern Apennines (Italy), *Phys. Earth Planet. Inter.*, *105*, 73–93, doi:10.1016/S0031-9201(97)00071-X.

Sarıbudak, M. (1989), New results and a palaeomagnetic overview of the Pontides in northern Turkey, *Geophys. J. Int.*, *99*, 521–531, doi:10.1111/j.1365-246X.1989.tb02037.x.

Sarıbudak, M., M. Sanver, A. M. C. Şengör, and N. Görür (1990), Palaeomagnetic evidence for substantial rotation of the Almacik flake within the North Anatolian Fault Zone, NW Turkey, *Geophys. J. Int.*, *102*, 563–568, doi:10.1111/j.1365-246X.1990.tb04582.x.

Satır, M., and H. Friedrichsen (1986), The origin and evolution of the Menderes Massif, W-Turkey: A rubidium/strontium and oxygen isotope study, *Geol. Rundsch.*, *75*, 703–714.

Scheepers, P. J. J., and C. G. Langereis (1994), Magnetic fabric of Pleistocene clays from the Tyrrhenian arc: A magnetic lineation induced in the final stage of the middle Pleistocene compressive event, *Tectonics*, *13*, 1190–1200, doi:10.1029/94TC00221.

Şenel, M., et al. (2001), Geological map of Turkey, scale 1:500,000, Maden Tetkik ve Arama Gen. Mudurlugu, Ankara, Turkey.

Şengör, A. M. C., and Y. Yilmaz (1981), Tethyan evolution of Turkey: A plate tectonic approach, *Tectonophysics*, *75*, 181–241, doi:10.1016/0040-1951(81)90275-4.

Şengör, A. M. C., D. Altıner, A. Cin, T. Ustaömer, and K. J. Hsu (1988), Origin and assembly of the Tethyside orogenic collage at the expense of Gondwana Land, in *Gondwana and Tethys*, edited by M. G. Audley-Charles and A. Hallam, pp. 119–181, Oxford Univ. Press, Oxford, U. K.

Shillington, D. J., N. White, T. A. Minshull, G. R. H. Edwards, S. M. Jones, R. A. Edwards, and C. L. Scott (2008), Cenozoic evolution of the eastern Black Sea: A test of depth-dependent stretching models, *Earth Planet. Sci. Lett.*, *265*, 360–378, doi:10.1016/j.epsl.2007.10.033.

Sinclair, H. D., S. G. Juranov, G. Georgiev, P. Byrne, and N. P. Mountney (1997), The Balkan thrust wedge and foreland basin of eastern Bulgaria: Structural and stratigraphic development, in *Regional and Petroleum Geology of the Black Sea and Surrounding Region*, edited by A. G. Robinson, pp. 91–114, Am. Assoc. of Pet. Geol., Tulsa, Okla.

Tatar, O., J. D. A. Piper, R. Graham Park, and H. Gursoy (1995), Palaeomagnetic study of block rotations in the Niksar overlap region of the North Anatolian Fault Zone, central Turkey, *Tectonophysics*, *244*, 251–266, doi:10.1016/0040-1951(94)00241-Z.

Tauxe, L., and D. V. Kent (1984), Properties of a detrital remanence carried by hematite from study of modern river deposits and laboratory redeposition experiments, *Geophys. J. R. Astron. Soc.*, *76*, 543–561.

Tauxe, L., and D. V. Kent (2004), A simplified statistical model for the geomagnetic field and the detection of shallow bias in paleomagnetic inclinations: Was the ancient magnetic field dipolar?, in *Timescales of the Paleomagnetic Field*, *Geophys. Monogr. Ser.*, vol. 145, edited by J. E. T. Channell et al., pp. 101–115, AGU, Washington, D. C.

Torsvik, T. H., R. D. Muller, R. Van der Voo, B. Steinberger, and C. Gaina (2008), Global plate motion frames: Toward a unified model, *Rev. Geophys.*, *46*, RG3004, doi:10.1029/2007RG000227.

Tüysüz, O. (1999), Geology of the Cretaceous sedimentary basins of the western Pontides, *Geol. J.*, *34*, 75–93, doi:10.1002/(SICI)1099-1034(199901/06)34:1/2<75::AID-GJ815>3.0.CO;2-S.

Tüysüz, O., and U. K. Tekin (2007), Timing of imbrication of an active continental margin facing the northern branch of Neotethys, Kargı Massif, northern Turkey, *Cretaceous Res.*, *28*, 754–764, doi:10.1016/j.cretres.2006.11.006.

Vandamme, D. (1994), A new method to determine paleosecular variation, *Phys. Earth Planet. Inter.*, *85*, 131–142, doi:10.1016/0031-9201(94)90012-4.

Van der Voo, R. (1968), Jurassic, Cretaceous and Eocene pole positions from northeastern Turkey, *Tectonophysics*, *6*, 251–269, doi:10.1016/0040-1951(68)90053-X.

Van Velzen, A. J., and J. D. A. Zijderveld (1995), Effects of weathering on single domain magnetite in early Pliocene marls, *Geophys. J. Int.*, *121*, 267–278, doi:10.1111/j.1365-246X.1995.tb03526.x.

Vasiliev, I., C. Franke, J. D. Meeldijk, M. J. Dekkers, C. G. Langereis, and W. Krijgsman (2008), Putative greigite magnetofossils from the Pliocene epoch, *Nat. Geosci.*, *1*, 782–786, doi:10.1038/ngeo335.

Vincent, S. J., M. B. Allen, A. D. Ismail-Zadeh, R. Flecker, K. A. Foland, and M. D. Simmons (2005), Insights from the Talysh of Azerbaijan into the Paleogene evolution of the South Caspian region, *Geol. Soc. Am. Bull.*, *117*, 1513–1533, doi:10.1130/B25690.25691.

Watson, G. (1983), Large sample theory of the Langevin distributions, *J. Stat. Plann. Inference*, *8*, 245–256, doi:10.1016/0378-3758(83)90043-5.

Whitney, D. L., C. Teyssier, Y. Dilek, and A. K. Fayon (2001), Metamorphism of the Central Anatolian Crystalline Complex, Turkey: Influence of orogen-normal collision vs. wrench-dominated tectonics on P-T-t paths, *J. Metamorph. Geol.*, *19*, 411–432, doi:10.1046/j.0263-4929.2001.00319.x.

Yalınız, K. M., M. C. Güncüoglu, and S. Özkan-Altıner (2000), Formation and emplacement ages of the SSZ-type Neotethyan ophiolites in central Anatolia, Turkey: Palaeotectonic implications, *Geol. J.*, *35*, 53–68, doi:10.1002/1099-1034(200004/06)35:2<53::AID-GJ837>3.0.CO;2-6.

Yılmaz, C., and R. Kandemir (2006), Sedimentary records of the extensional tectonic regime with temporal cessation: Gumushane Mesozoic Basin (NE Turkey), *Geol. Carpathica*, *57*, 3–13.

Yılmaz, C., C. Şen, and A. S. Özgür (2003), Sedimentological, paleontological and volcanic records of the earliest volcanic activity in the Eastern Pontide Cretaceous volcanic arc (NE Turkey), *Geol. Carpathica*, *54*, 377–384.

Zijderveld, J. D. A. (1967), A. C. demagnetization of rocks: Analysis of results, in *Methods in Palaeomagnetism*, edited by D. W. Collinson, K. M. Creer, and S. K. Runcorn, pp. 254–286, Elsevier, Amsterdam.

Zimmerman, A., H. J. Stein, D. Hannah, D. Kozelj, K. Bogdanov, and T. Berza (2008), Tectonic configuration of the Apuseni–Banat–Timok–Srednogorie belt, Balkans-South Carpathians, constrained by

high precision Re–Os molybdenite ages, *Miner. Deposita*, *43*, 1–21, doi:10.1007/s00126-007-0149-z.

J.-C. Hippolyte, CEREGE, UMR 6635, Université Aix-Marseille III, CNRS, BP 80, Europôle Méditerranéen de l'Arbois, F-13545 Aix-en-Provence CEDEX 4, France.

N. Kaymakci, Department of Geological Engineering, Faculty of Engineering, Middle East Technical University, İnönü Bulvarı, 06531- Ankara, Turkey.

C. G. Langereis, Paleomagnetic Laboratory Fort Hoofddijk, Department of Earth Sciences, Utrecht University, Budapestlaan 17, NL-3584 CD Utrecht, Netherlands.

M. J. M. Meijers, Paleomagnetic Laboratory Fort Hoofddijk, Dept. of Earth Sciences, Utrecht University, Budapestlaan 17, 3584 CD Utrecht, Netherlands. (meijers@geo.uu.nl)

R. A. Stephenson, School of Geosciences, University of Aberdeen, Meston Building, King's College, Aberdeen, AB24 3UE, UK.

D. J. J. van Hinsbergen, Physics of Geological Processes, University of Oslo, Sem Sælands Vei 24, NO-0316, Oslo, Norway.